Delft University of Technology

Graduation project report

Is under-base filling necessary?

Assessing behaviour of partially installed suction caisson

Author:
Astha Sharma (5606799)

Supervisors:
Prof. K.G.Gavin
Dr. M.A.Cabrera
Ir. Erik ter Horst
Dr. Weiyuan Zhang

June 29, 2023

Contact Information

Astha Sharma (student)
TU Delft

Prof. K.G.Gavin
TU Delft

Dr.M.A.Cabrera
TU Delft

Ir. Erik ter Horst
Deme

Dr.Weiyuan Zhang
Deme

Acknowledgment

I would like to extend my sincere gratitude to my supervisors, Prof. Ken Gavin and Dr. Miguel Cabrera, for their invaluable guidance and unwavering support throughout the entirety of my thesis. Their expertise and assistance were truly instrumental in shaping the direction of my research. I am also deeply grateful to my supervisor from Deme SPT Offshore, Dr. Weiyuan Zhang, for providing insightful perspectives and motivation that greatly enriched the thesis process. I would also like to express my heartfelt appreciation to Ir. Erik ter Horst for his diligent efforts in keeping me well-informed about all the official procedures during my thesis period at Deme SPT Offshore.

Furthermore, I am immensely thankful to Francisco da Silva Pereira and Prof. Conleth O'Loughlin from the University of Western Australia for their invaluable support in conducting the centrifuge experiments. Their expertise and collaborative spirit greatly contributed to the success of my research. I would also like to acknowledge Deme SPT Offshore, particularly Ir. Andrew Harding, for their generous funding that made it possible for me to conduct the experiments and travel to Australia. The support and teamwork from the entire Deme SPT Offshore team made my entire thesis journey easy and enjoyable, and for that, I am truly grateful.

Lastly, I want to express my heartfelt appreciation to my family and friends for their unwavering support throughout this journey. Their encouragement and understanding played a crucial role in my accomplishments, and I am forever grateful for their presence in my life.

Abstract

In the past decade, suction caissons have emerged as a preferred offshore foundation solution for wind turbines due to their silent installation process and potential for recyclability. However, there has been growing speculation regarding the necessity of under base filling, which involves filling the gap between the top plate of the suction caisson and the seabed. Some experts have suggested that under certain conditions, this under base filling may not be required at all. Furthermore, concerns have been raised about the efficacy of under base filling in achieving full contact between the top plate and the seabed, as it has been observed that gaps may persist even after the filling is applied. Consequently, doubts have been cast on the overall need for under base filling.

However, there is limited research focused on understanding the behavior of water plugs in the absence of under base filling, at different loading conditions (Compression , tension , cyclic etc.). This knowledge gap motivates this thesis study, which aims to investigate the behavior of water plugs specifically in dense sand samples, as sand is considered more critical compared to clay in terms of its variablity in drainage conditions that can influence the foundation's performance. To achieve this, a series of centrifuge tests were conducted on suction caissons that were partially installed and some fully installed.

The results of the experiments shed light on the role of under base filling in different loading scenarios. Under monotonic compressive loading at higher rates, it was observed that under base filling played no significant role in the load transfer . Both the caissons with and without under base filling exhibited similar load transfer mechanisms, indicating that filling the gap may not be necessary in such loading conditions. Additionally, under tension loading, it was found that under base filling had little to no effect on the development of tensile capacity.

By expanding our understanding of the necessity and effectiveness of under base filling, this study contributes to the ongoing discussion surrounding suction caisson design and installation practices for offshore wind turbine foundations.

Table of Contents

Nomenclature

α	Dimesionless factor [-]
δ	Interface friction angle [°]
σ'_v	Vertical effective stress $[N/m^2]$
A_p	Foundation wall tip area $[m^2]$
A_{shaft}	Curved shaft surface area $[m^2]$
A_{so}	Caisson outer perimeter $[m]$
A_s	Caisson inside and outside surface area $[m^2]$
f	Unit skin friction resistance $[N]$
F_{sr}	Soil resistance $[N]$
k	Coefficient of earth pressure [-]
k_f	Empirical coefficient relating qc to unit skin friction resistance [-]
k_p	Empirical coefficient relating qc to end bearing [-]
N_c	Dimensionless bearing capacity factor [-]
q	Unit end bearing resistance $[N]$
$q_{c,l}$	Cone tip resistance at embedment depth l $[N]$
$q_{c,z}$	Cone tip resistance at depth z $[N]$
Q_d	Total caisson resistance $[N]$
Q_f	Total friction resistance along sides of caisson $[N]$
Q_p	Total end bearing resistance at caisson tip $[N]$
s_u	Soil undrained shear strength $[N/m^2]$

Chapter 1

Introduction

This chapter aims to provide a comprehensive overview of the main component of the thesis topic, focusing on its background. It starts by discussing the growing need for renewable energy and the significance of geo-technical structures in achieving sustainable energy goals. The chapter intends to establish the foundation concepts that are crucial for understanding the research objectives and problems to be addressed in the subsequent chapters.

1.1 Energy need and history

The Ukraine-Russia conflict have led to a massive energy crisis in Europe . There has been a rise of 600% in European gas prices, resulting in a decline of natural gas demands. It is the result of declining production due to deposits running dry. Also, one of the major reasons is, supply restrictions from the eastern countries. This whole situation has led to a shift towards renewable energy resources (World Economic Forum (2022)). While today it is the need, it all started with the Kyoto protocol of 1997. One of the reasons behind the birth of renewable energy industry. It led to 160 countries coming together to conquer the concern over the security of energy supply by boosting renewable energy. Following up, recently the European Union presented the aim to be a net-zero emission continent by the year 2050 (European Commission (2022)), and the way to achieve it is by increasing renewable energy production.

There are multiple options available for the generation of renewable energy, be it solar energy, wind energy, hydro, or bio-energy. Each source contributes to solving the problem of rising greenhouse emissions. Amongst all these sources, wind and hydro-energy account for more than two-thirds of the total electricity generated from renewable sources. Also, In 2020 renewable energy sources contributed to 37.5% of the energy demand in Europe(Eurostat (2020)). Hence, making it a rising industry with a lot more potential.

Land availability is a significant concern when it comes to structures associated with renewable energy. As the global population continues to grow at a rate of 0.9%, (Worldometer (2023))the amount of livable space is gradually decreasing. This is where offshore wind energy emerges as a solution, utilizing the vast expanses of the Earth's oceans. Offshore energy not only maximizes the utilization of available space but also offers several additional

advantages. For instance, offshore locations often experience superior wind yield, resulting in higher energy production. Furthermore, the restrictions on turbine size are minimal in offshore environments, allowing for the deployment of larger and more efficient turbines.

Coming to the history of offshore renewables, the first offshore wind turbine, located in vindeby, Denmark, was constructed in 1991. Later in 2001, vindeby became an offshore wind farm with 11 wind turbines generating 5MW in total (Ørsted (2020)). From 5MW to now, the largest wind farm located in the UK will produce a total of 1.3GW of energy by using 165 wind turbines. This wind farm will be fully operational by 2030 and will be a significant step towards a renewable future(Ørsted (2022)).

The main component used for Offshore renewable energy production is a Turbine structure. Even though the name includes offshore, its production has almost nothing to do with waves and currents. Energy production is only relevant to wind and sun. The wind produced by uneven heating of the earth's surface helps rotates the turbine plates and then converts the kinetic energy into electrical energy. Wind blowing over the turbine blades causes them to rotate, which in turn spins the rotor hub. The rotor hub is connected to a motor that drives an electricity generator(Kaldellis (2022)). This process requires the use of a large structure called turbine tower. The dimensions of a wind turbine in Europe range between 50m to 115m in blade length and structure height of 250m – 280m (Niklas (2022)). This large turbine structure surely requires a sturdy platform. So, this is where the offshore geotechnical structures come to play.

The offshore geotechnical structures are required to support the wind turbines. Hence, various types of support structures are present, depending on load and soil conditions. Noting that these structures require to resist the most versatile loading conditions like wind loads, wave loads, storm loads etc., a proper design of foundations plays cardinal role. The load applied to the turbine can be a combination of horizontal load, vertical (compression, tension) load, and the moment. To resist these loads mainly three types of foundation are used around the globe: Gravity foundation, Monopile, and suction caisson. The focus of thesis is around suction caisson hence following section provides additional details about this type of foundation.

1.2 Suction caisson and history

Suction caissons are also referred to as intermediate foundations because they are installed at a depth that falls between shallow and deep foundations (Senders (2008)) (embedment depth ranging approximately 4m to 30m). These upside-down bucket-shaped structures can be used as mono, tri, or tetrapod foundations and are installed using self-weight penetration and suction, resulting in a less noisy process. Their depth of installation lies somewhere between that of gravity foundations and piles. Different types of offshore wind turbine foundations are illustrated in Figure 1.1(The Figure don't include some new offshore foundations)

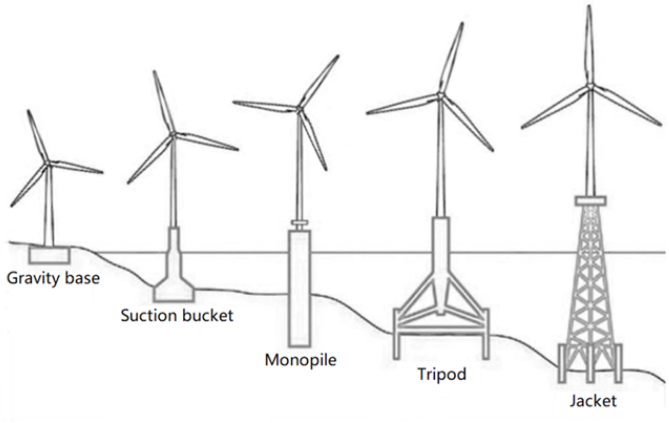

Figure 1.1: Different types of Offshore foundation (M. Xie & Lopez-Querol (2021))

One of the key advantages of suction caissons is their silent and efficient installation, which has a lower environmental impact than other foundation types. Despite this, 80% of offshore turbines still use mono-piles, even though suction caissons offer significant advantages over other offshore foundation types and have the potential for further growth. According to DNV Energy Transition Outlook 2022 (DNV (2022)), offshore energy produc-

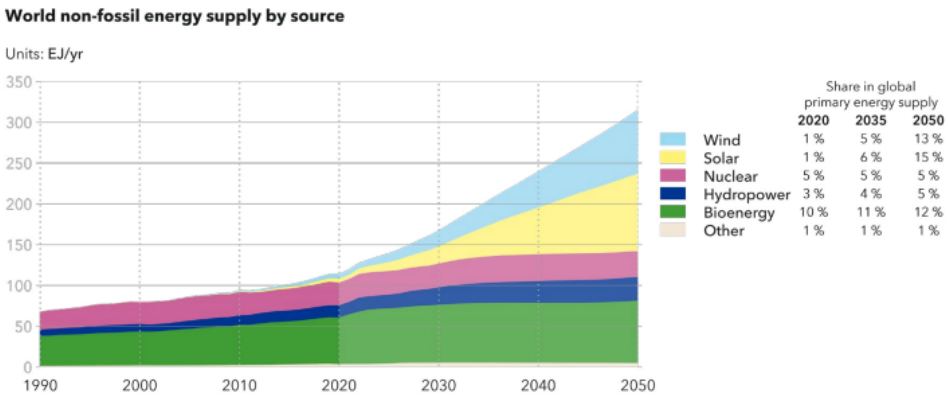

Figure 1.2: Global renewable Energy production and Projection(DNV (2022))

tion has consistently shown exponential growth, surpassing other renewable energy sources as illustrated in Figure 1.2 and 1.3. This growth trajectory indicates an increasing demand for support structures, including suction caissons. Although the development of suction caissons as a support foundation has taken time to perfect, it is now expected to experience accelerated growth. The aim of this thesis is to address and comprehend one of the challenges associated with suction caisson installation, as mentioned in Section 1.3, and propose a suitable solution.

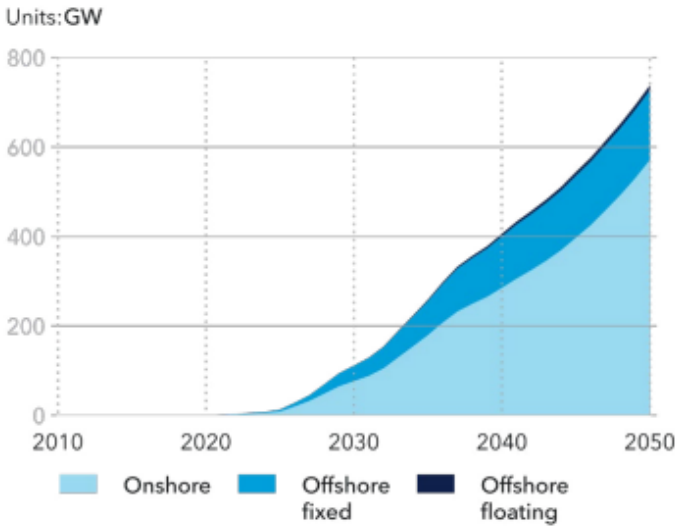

Figure 1.3: Global wind energy production and projection (DNV (2022))

1.3 Drawbacks and benefits

The multiple design challenges regarding suction caisson can be listed as follows(G. S. Randolph M. (2017)):

1. The construction process is more complex compared to mono-piles (As Suction caisson require more machinery for there installation).
2. Absence of end bearing capacity in some soil cases.
3. These foundations are susceptible to soil vibrations, where even small vibrations can have a significant impact on their strength.
4. Failure conditions like plug heave, reverse end bearing, and soil piping can be observed in this type of foundation.

Nevertheless, ongoing research is exploring potential solutions for all these concerns. Although this type of foundation presents some economic and engineering challenges, it also offers numerous advantages that are not easily available with any other foundation in the market. Some of the key benefits of suction caissons, as outlined in Lembrechts (2013) and OWA (2019), are:

1. Offshore vessel time can be reduced by installing these foundations as a single structure.
2. The use of a noise-free suction installation technique minimizes harm to marine life, eliminates the need for noise mitigation equipment, and allows for flexibility in scheduling.

3. The foundation's wide area of coverage results in little or no seabed preparation, reducing costs further.

4. This offshore foundation renewability and replaceability is a significant advantage. It can be removed safely at the end of its life by applying over pressure, making it an environmentally friendly option.

5. The installation technique using under pressure generates minimal emissions.

6. Suction-assisted installation provides flexible control for positioning the suction caisson on the seabed. Using under pressure and over pressure, the caissons can be installed with high precision.

7. The installation technique also makes this foundation suitable for multiple soil types.

Given that the use of these foundations is a relatively recent development, there remains a great deal of potential for further research in this area. Nevertheless, despite certain concerns, the numerous advantages provided by suction caisson foundation far outweigh the drawbacks, especially when considering the ongoing research effort to alleviate these issues. Consequently, it seems probable that these foundations will come to show more presence in the market within the next few years thanks to their environmentally friendly installation process and adaptability to a range of soil strata.

1.4 Chapter guide

Chapter1 Introduction : This chapter provides an in-depth understanding of suction foundations, including their historical development and the design challenges encountered during their implementation. Additionally, it highlights the advantages of suction caisson foundations compared to other available foundation types.

Chapter2 Literature Review: In this chapter, the necessary background knowledge for the research is presented. It covers the installation process of suction caissons, discusses the concept of under-base filling, and concludes with a problem statement that outlines the research questions to be investigated.

Chapter3 Physical Modelling: This chapter focuses on the methodology employed to address the research questions. It provides comprehensive details about the experimental setup and the procedural approach taken during the investigation.

Chapter4 Results and Discussion: The findings of the research are presented in this chapter, accompanied by detailed analysis and interpretation. The results are examined in relation to the research questions, enabling their conclusive answers.

Chapter5 Conclusion: This chapter presents the overall conclusions derived from the conducted research. It summarizes the key findings, highlights significant contributions, and offers insights into the implications of the study.

Chapter6 Recommendations: The final chapter of the thesis provides recommendations for future studies to enhance the scope and understanding of the topic. It suggests potential avenues for further research and improvements that could be made to advance the field.

Chapter 2

Literature review

A suction foundation can be described as a large steel cylinder, open at the bottom and covered from the top. The suction foundations are known by different names depending on their purpose, like suction caissons, suction anchors, suction buckets, etc. The name of this offshore foundation comes from the installation method. After initial penetration under its self-weight, the caisson is embedded into the seabed to target depth by creating negative pressure inside the caisson, and the resultant pressure differential across the top plate effectively pushes the caisson into the seabed.

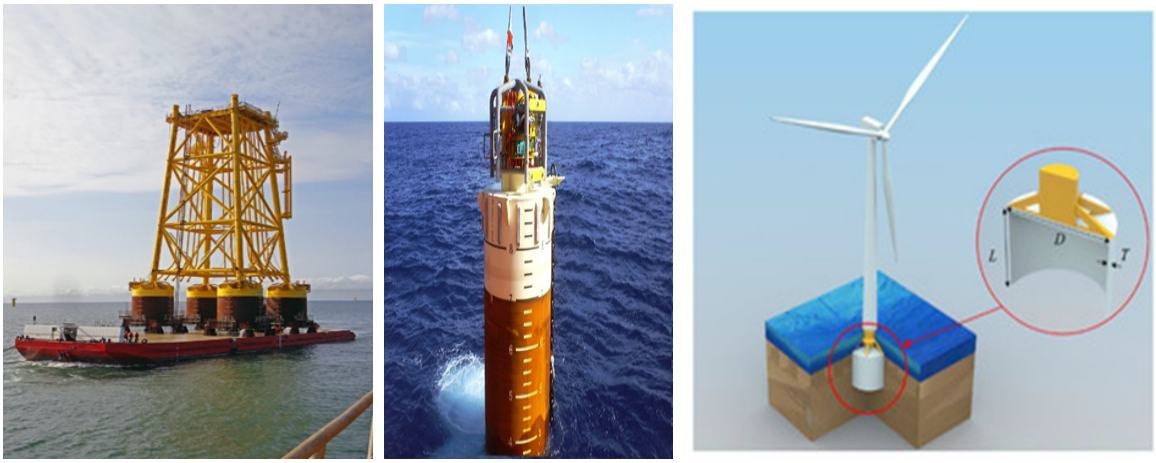

Figure 2.1: Suction bucket foundation (left), suction anchors (middle), Suction Caisson (right)(L. Xie et al. (2020))

The usage of these foundations spreads over many sectors. It can be used as a foundation structure for the wind turbine, oil, and gas extraction structures. On other hand, it can also be used for mooring purposes, in this case it is commonly referred to as a suction-installed anchors.

2.1 Installation

The installations technique of this foundation is divided into two main phases:

1. Self-weight penetration
2. Suction-induced penetration.

During installation of foundation, the steel caisson penetrates the seabed under the influence of its self-weight. The depth of penetration depends on the characteristics of the soil and comes to a halt when the soil resistance balances the weight of the caisson. At this point, water is pumped out of the system, generating a differential pressure that drives further penetration of the caisson into the seabed until the target depth is reached. These phases are depicted in Figure 2.2 . The assessment of soil resistance (F_{sr}) can be achieved through two principal methods:

1. CPT based method
2. Classical bearing Capacity theory (α,β)

The CPT is considered more reliable as it is based on values derived from in-situ conditions. However, the classical bearing capacity method can help to provide a double check to the q_c values. Also, in the cases where it's hard to perform the CPT test than the bearing capacity method is the one to rely on. Bearing capacity method is also easy to calculate as we only need s_u as well as q_c is required.

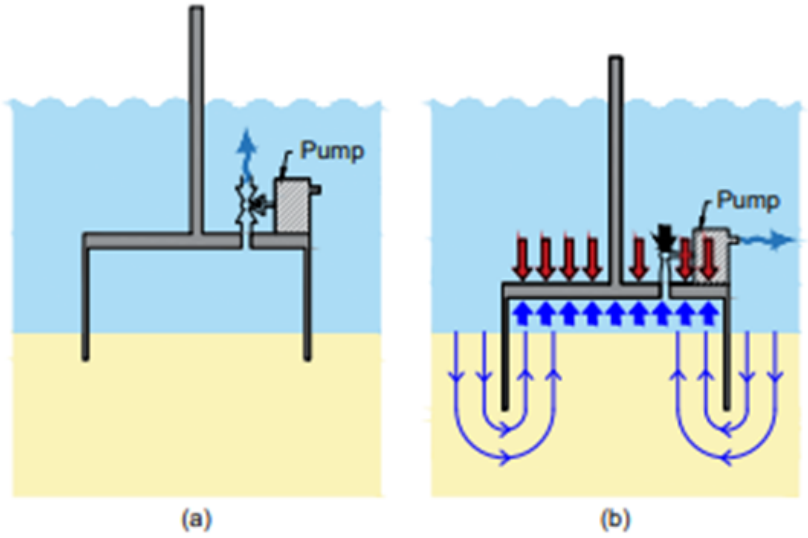

Figure 2.2: (a) Self weight penetration (b) suction installation(da Silva Pereira et al. (2022))

1. CPT Based method

   The CPT method uses the insitu data to find out the soil resistance profile. It is considered more accurate than the other site investigation methods as it includes the

use of cone resistance(qc). The resistance is assessed based on the (DNV (1992)) method where $q_{\{c,l\}}$ cone tip resistance at caisson embedded depth l and $q_{\{c,z\}}$ means one tip resistance at depth z below seafloor .The formula can be written as follows:

$$F_{sr} = A_p k_p q_{\{c,l\}} + A_s i \int k_f q_{\{c,z\}} dz + A_{so} \int k_f q_{\{c,z\}} dz \tag{2.1}$$

2. Classical bearing capacity method

   Unlike the CPT-based method, this approach provides distinct ways of computing soil resistance for sand and clay. While the universal equation remains constant, the coefficient values differ depending on the drainage conditions. The soil resistance equation is formulated as follows(G. S. Randolph M. (2017)):

$$F_{sr} = Q_d = Q_f + Q_p = f A_s + q A_p \tag{2.2}$$

   For undrained soil response, q and f can be calculated as follows:

$$f = \alpha \ s_u \qquad \text{and} \qquad q = N_c s_u \tag{2.3}$$

Where the values of dimensionless adhesion factor α are applied in accordance with DNV (2007) and dimensionless bearing capacity factor N_c are applied in accordance to ISO (2016).

2.1.1 Self weight installation

In the installation process, the caisson is gradually lowered and allowed to be installed solely under the influence of its own weight. The classical bearing capacity method can be used to calculate the resistance for self weight penetration by adding the outer friction resistance, inner friction resistance, and end bearing on annulus. This approach is documented in references Houlsby (2005b) and Houlsby (2005a).

2.1.2 Suction penetration

To continue installing suction caissons to greater depths, external force is needed since the soil resistance increases with depth. Suction pressure is applied as this external force, resulting in a nearly noise-free installation compared to dynamic loading.

The suction pressure required to achieve the desired penetration depends on the soil type and caisson dimensions. To ensure proper installation, the suction pressure applied must be greater than the soil resistance (Kay et al. (2021)), which can be calculated using the equation outlined in Houlsby, 2005b and Houlsby (2005a).

2.1.3 Retrieval and removal

Apart from installation, it is also crucial to consider retrieval and removal when assessing the suitability of suction caissons as foundations. In cases where the desired target penetration is not achieved due to various factors, such as poor soil conditions or other

unforeseen circumstances, overpressure may be required to extract the foundation, reposition it, and reinstall it. Similarly, removal of the foundation may be necessary when it has reached the end of its useful life or when the site needs to be cleared. In such cases, overpressure is often used as a more cost-effective method compared to excavating the soil around the foundation perimeter and cutting the foundation steel. This process also results in fully intact extraction, leaving no debris on the seabed, and the extracted metal can be recycled for other purposes. As a result, suction caissons are one of the most sustainable forms of offshore foundations available.

The difference between installation and retrieval removal is that in case of installation analysis is performed to find the under pressure while in case of retrieval and removal, assessing of over pressures is required.

The calculation of over pressure can be carried out by evaluating the resistance offered by the foundation. It should be noted that end bearing at the tip level is considered insignificant since no passive suction exists beneath the top plate when the vent is kept open. One form of resistance is provided by the weight of the suction caisson, which means that the applied over pressure must be sufficient to overcome the weight of the foundation.

2.2 Types of failures

Suction caissons are cylindrical structures used to support offshore wind turbines and oil rigs. These structures are embedded into the seabed by applying suction pressure to the interior of the caisson, hence, they are susceptible to several types of failures(G. S. Randolph M. (2017),Kay et al. (2021)).

1. Compression failure:

   Compression failure is the failure mode in which the suction caisson experiences excessive stress under compressive loads, leading to failure. The soil around the caisson may undergo excessive deformation and ultimately lose bearing capacity, causing the suction caisson to fail. The failure can occur due to a combination of factors, including the undrained strength of the soil, the geometry of the suction caisson, and the magnitude of the compressive load.

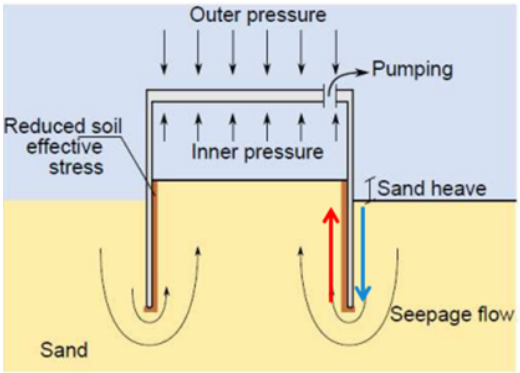

Figure 2.3: Pressure distribution during Installation

2. Pullout failure:

   Pullout failure occurs when the soil around the suction caisson is unable to withstand the tensile forces imposed on it during the pulling action. The failure can occur due to several reasons, such as the absence of effective soil confinement, soil liquefaction, or the suction caisson's unsuitability for the soil type. In this mode of failure, the suction caisson loses its adhesion to the soil, leading to its pullout.

   (a) Plugged failure:

   Plugged failure occurs when the suction caisson is blocked by soil, reducing its suction capacity. This type of failure can be caused by soil particles entering the caisson during the installation process, which leads to clogging of the suction ports. The clogging of suction ports leads to a reduction in suction capacity, which, in turn, reduces the suction caisson's bearing capacity, leading to failure.

   (b) Coring failure:

   Coring failure occurs when the soil within the suction caisson is extruded out of the caisson during the installation process. This type of failure is mainly caused by the high shear stress exerted on the soil by the suction caisson during the installation process. The soil's extrusion results in the formation of a cavity around the caisson, reducing its bearing capacity and leading to failure.

   (c) Leaking failure:

   Leaking failure is the type of failure in which the suction caisson loses suction due to the soil's seepage into the caisson's internal cavity. This type of failure occurs when the soil around the suction caisson is poorly consolidated, leading to seepage of water and soil particles into the caisson. The suction caisson's loss of suction results in reduced bearing capacity, leading to failure.

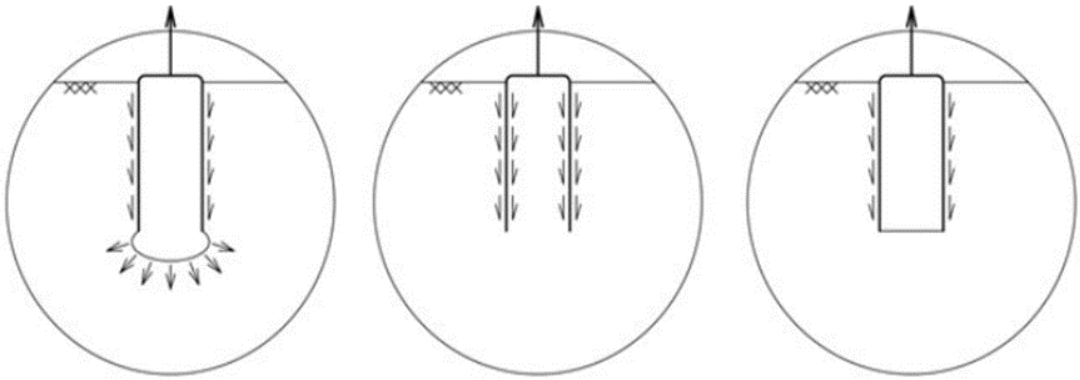

Figure 2.4: Typical pull out failure in suction caisson - Plugged, Coring , Leaking , (G. S. Randolph M. (2017))

2.3 Additional mechanism

Under field conditions, caissons are often exposed to tensile loading, either directly when used for a floating structure or through the application of high overturning moments. When the rate of tensile loading is such that undrained conditions occur, a negative pore pressure or suction is generated between the top plate and the soil plug. This creates an opportunity for reverse end bearing to occur. The development of reverse end bearing is illustrated in Figure 2.5, where σ_{zo} represents outer vertical stresses and σ_{zi} represents the vertical stress inside the caisson. The difference in stresses between the inner and outer regions leads to the generation of negative pore pressures.

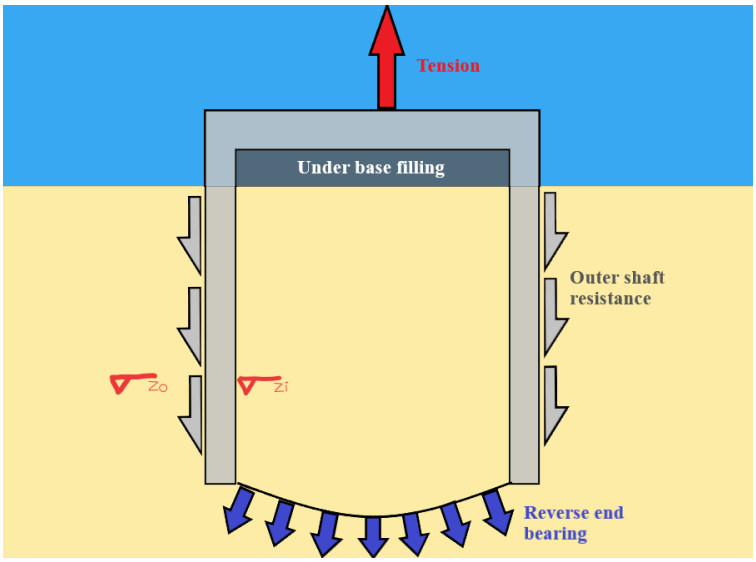

Figure 2.5: Reverse end Bearing

2.4 The gap between top plate and seabed

In this chapter, the focus is on providing an understanding of why a gap may exist between the top plate of a structure and the seabed, as well as the potential implications of such a gap. The chapter aims to provide readers with a clear overview of the factors that contribute to the creation of this gap.

2.4.1 Why the gap is kept?

The gap between the top plate and the seabed has two reasons. The first one is intentional, not dependent on soil type. The second one, which is dependent on soil properties, can occur due to various reasons like plug heave, erosion, etc.

As the contact between the top plate and the seabed is considered crucial to mobilize the end-bearing capacity. This contact helps transfer loads from the top plate to the seabed, resulting in additional resistance. However, the seabed is typically not uniform and can have undulations or inclinations due to water currents or geological conditions. These seabed

irregularities can lead to several issues, one of which is the risk of losing contact between the top plate and the seabed. According to some hypothesis, this loss of contact can significantly reduce the suction foundation's bearing capacity (Sturm (2019)) and make it susceptible to tilting failure due to horizontal loading. To address the problems discussed above, the

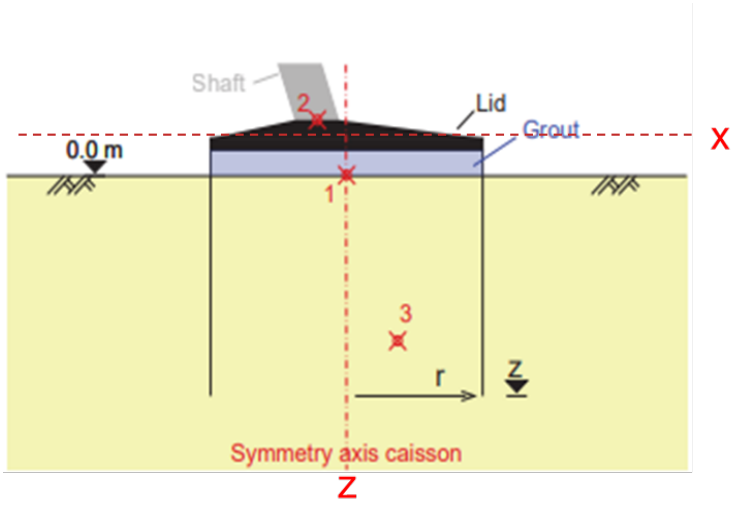

Figure 2.6: Typical setup of suction pile with under base filling, (Sturm (2019))

suction foundation design is amended by selecting the penetration depth to ensure that seabed undulations do not affect the bearing capacity. This is achieved by leaving a gap of 0.5m to 1m between the seabed and the top plate. To maintain the end-bearing capacity, this gap is filled with low-strength under base filling.

2.4.2 Why the gap arises?

The existence of a gap between the top plate and seabed may not always be a result of deliberate actions. There are several other situations that can lead to its formation, which are outlined below.

1. Displacement due to installation effect

   While the suction pile is driven into the seabed using suction pressure, it is bound to displace the equal volume of soil. This displacement results in heave. Tran et al. (2004) conducted a PIV (Particle image velocimetry) study to investigate the amount and area of displacement. It was found that most displacements occur in a triangular-shaped region near the suction caisson. While the middle area remains almost unaffected.

   As shown in the figure 2.7 the displacement is seen around the suction caisson walls. It can be concluded that this amount of displacement hardly affects the relative density of the soil. Hence, causing no significant problems. However, it can lead to generation of an empty space in between.

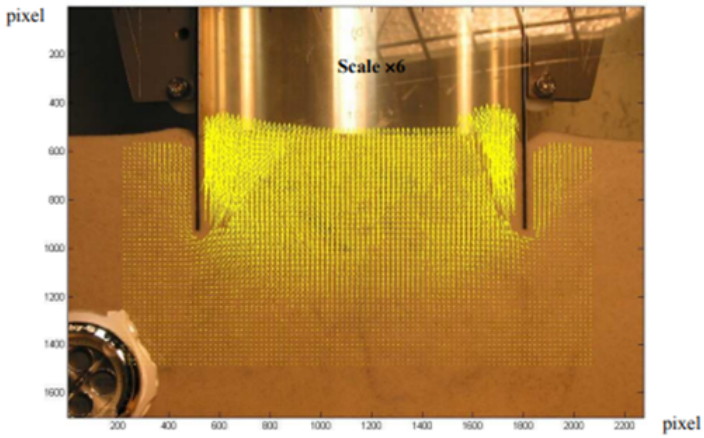

Figure 2.7: Displacement field as obtained through PIV analysis during suction installation in the centrifuge. (Tran et al. (2004))

2. Plug heave due to seepage inflow

   In this case, the heave is caused due soil loosening. As shown in Figure 2.8, it caused due to seepage inflow, hence causing an increase in the volume of the soil plug. This phenomenon is observed mostly above the critical suction pressure. If the pressure gradient inside the soil plug remains below the critical gradient, positive stress will remain effective hence no change can be observed in the relative density of the soil plug. But once the critical gradient is achieved, the plug liquifies and increases in volume.

   This phenomenon can later be responsible for making a gap. As, once the gradient is removed, the soil plug is bound to settle down. Hence giving rise to a gap between the top plate and seabed. Trans (Tran et al. (2004)) investigated the loosening effect by observing the seepage flow. He used the fact that when the sand plug loosens, its permeability also changes, resulting in differences in the amount of seepage. He also found out (using PIV) that the sand loosens more adjacent to the caisson wall than towards the middle of the plug due to the shorter hydraulic path. Using Darcy's law on trans-related discharge and permeability also helped him in finding the plug heave due to the installation effect. The change in permeability to collective effect was found to be to the factor of 1.5 to 2.

3. Erosion due to water pulses under to plate

   According to Sturm (2019), many times there can be the possibility of vertical cyclic load in an offshore environment. Due to the the water plug below the lid can become exposed to continuous pressure pulses. This can can trigger a local piping failure along the walls of the suction caisson. This phenomenon is one of the reasons filling the gap is important.

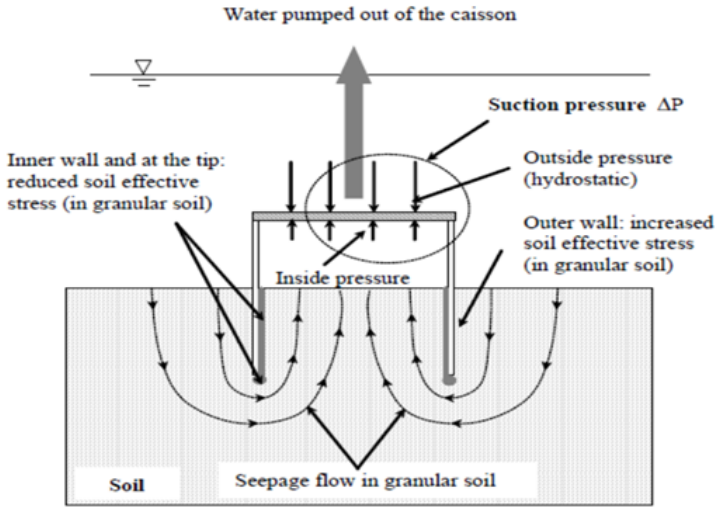

Figure 2.8: The upward seepage flow due to suction, Tran (2007)

2.5 Under base filling

Depicted in Figure 2.6, the implementation of a low strength under base filling to fill the area between the top plate and seabed serves a vital purpose. This filling is essential for achieving complete contact with the seabed, which cannot be accomplished solely by the lid (as explained in section 2.4.2). Consequently, including under base filling has become a fundamental design principle for suction caisson foundations. Nevertheless, it is conjectured that in certain cases, this practice may merely increase the project's cost without contributing to the mobilization of any resistance. This speculation arises from the inability to verify if the under base filling adequately fills the gap between the top plate and seabed. There is a significant possibility that the desired contact is not achieved. However, this speculation requires further investigation and solid experimental evidence.

2.5.1 Importance of under-base filling

The significance of this under base filling can be summarized in the following section.

1. To avoid further penetration of the caisson . If one assume the scenario of no gap, further settlement of the suction caisson is possible under many circumstances. As the compressive load such as turbine load is applied days after the installation of the suction foundation. It will lead to the generation of excess pore water pressure, which will dissipate over time (G. S. Randolph M. (2017)). Hence leading the settlement of the suction caisson, can lead to an increase in design penetration depth.

2. To obtain uniform soil stresses across the foundation(G. S. Randolph M. (2017)). This is one of the main reasons behind under base filling. However, there is no possible way of assuring that the under-base filling is fulfilling this purpose. It is highly possible that the filling was done unevenly.

3. As mentioned in section 2.4.2 , due to cyclic vertical loading, the water cushion below the lid is exposed to continuous pressure pulses, which can trigger a local pipping failure along the skirt (-(Tran et al. (2004)). This phenomenon can be avoided by filling the gap and restricting the moment of the lid as much as possible.

4. Assuming that the under base filling is done uniformly, it also serves to avoid the possibility of differential settlements (Sturm (2019)). Which can be one of the threats if the water plug is left. In the case of the inclined seabed, the drainage path length can be different, hence may result in differential settlement of the caissons.

5. Lack of under base filling can also cause local stresses and moments over the lid, Which can be avoided by creating a thicker and sturdier lid. (Sturm (2019))

If the above-mentioned problems could be solved without under-base filling, then it can make the suction foundation way less expensive and more feasible. It is assumed that the main concern is the development of end bearing capacity from top plate contact and if this is achieved, it can be possible to eradicate under base filling in many cases.

2.5.2 When under base filling can be avoided

There can be specific circumstances or specific arrangements which can help in avoiding the under base filling. These cases are presented as follows:

1. If sufficient stiffness and vertical capacity can be demonstrated through caisson wall resistance alone. This may be the case if sustained tensile loads are governing. As in the case of tensile load end bearing capacity does not play much role. It is mostly dependent on skin friction and reverses bearing capacity (passive suction). Hence, contact between the top plate and the seabed is not a major concern. However, it is suspected that the presence of a water plug can result in faster dissipation of the passive suction generated due to the uplift pressure (Mana et al. (2013)). This area is subject to further research.

2. If sufficient (differential) settlement of the substructure can be accepted until the necessary load-transfer capability is achieved, and the stiffness is acceptable in the meantime. This may affect both the foundation tolerances and the structural design of the caissons and substructure(OWA (2019)).

3. If contact between the top plate and soil can be ensured by alternative means. For example, two methods proposed by the industry consist of (1) using a double top-plate, and (2) using a water jetting and slurry suction system. Although both alternatives have their shortcomings. The main disadvantages of using structural and jetting systems are, that the soil which is in contact with the structural components is soft, and the stresses in the lid may be concentrated to a few points only. (Sturm (2019))

4. If load transfer through the water-filled voids can be demonstrated for short-duration loads while not compromising any other load transfer or structural requirement. This may be possible for low permeability soils. Reliable sealing of all openings in the top plate after the suction installation would be required for the lifetime of the structure.

However, in case of permeable soils the water seepage through soil can result in reduction of pressure and hence losing the bearing capacity. This is a matter of research and if it can be avoided for permeable soil as well then, the under base filling can be avoided in many cases.

2.6 Problem statement

Despite the ongoing debate surrounding the necessity of under-base filling in the area between the top plate and seabed for suction caissons, there is a significant research gap regarding the behavior of water plugs under various loading conditions and the efficacy of alternative methods for ensuring contact between the top plate and soil without employing under-base filling. Additionally, there is a lack of comprehensive studies on load transfer through water-filled voids in permeable soils and the potential of demonstrating adequate stiffness and vertical capacity solely through caisson wall resistance, thereby eliminating the need for under-base filling. Addressing these research gaps can provide valuable insights into the feasibility of under-base filling-free suction caissons and potentially alleviate the high cost associated with under-base filling.

To bridge the aforementioned research gap, it is crucial to thoroughly understand the problem. Before delving into the issue at hand, a comprehensive comprehension of the foundation's fundamentals is necessary (Also mentioned in section 2.1). The suction foundation resembles an inverted bucket, and its installation involves creating a pressure difference through suction. The installation process consists of two stages: self-weight installation and suction installation. During the self-weight installation phase, the foundation is lowered by its own weight until the desired depth is achieved through self-weight penetration. In the subsequent suction installation stage, a pump connected to a valve on the top plate applies suction pressure to achieve the desired depth.

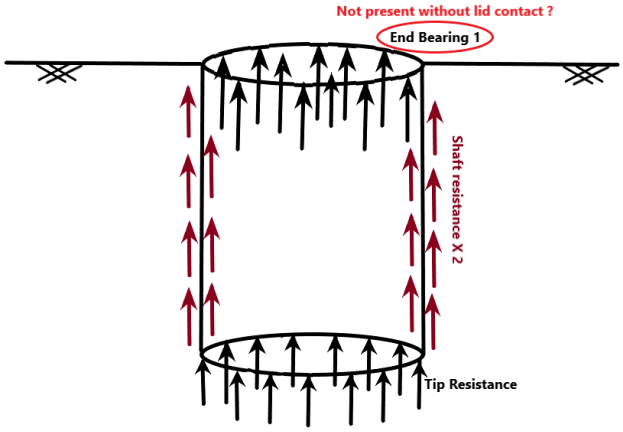

Figure 2.9: Different types of Resistance mobilized in caisson

However, to mitigate potential tilting caused by an uneven seabed, pumping limitations,

heave, and other factors, it is common practice to avoid complete contact between the seabed and top plate during penetration. As the pump approaches the seabed, soil or mud may be extracted, leading to pump malfunction and hindering the achievement of full contact. Consequently, attaining complete contact without under-base filling the gap between the top plate and seabed becomes challenging, despite its necessity to achieve the desired end bearing capacity. Furthermore, the cost associated with under-base filling is a significant concern, as it escalates the overall project expenses, including the additional vessel time required for filling. Hence, it is imperative to investigate the behavior of suction caissons without under-base filling the gap to ascertain whether omitting under-base filling will substantially impact the suction pile's capacity in certain scenarios.

The focus of this thesis is solely on the sandy seabed scenario as it is deemed more critical than a clayey seabed. Unlike clayey soil, which typically exhibits predominantly undrained behaviour, the water gap should not pose any capacity problems for the suction caisson. However, in the case of sand, the soil response is less predictable, necessitating further research. Figure 2.9 represents the a visual depiction of the problem statement.

2.7 Research questions

1. How the mobilized resistance of a suction caisson differs between a suction caisson that is partially and a suction caisson that is fully installed with the underlying soil, under monotonic compression and tensile loading?

2. What are the effects of loading rate after installation of a suction caisson i.e not in contact with the underlying soil?

It is also deemed important to mention any other additional findings that can be made using the test data. So, that the full utilization of the data obtained could be done.

2.8 Strategy and methodology

To answer the research questions, it is necessary to examine the behavior of water plugs under different loading conditions, which can be effectively achieved through physical modeling . However, creating a full-scale model for this purpose is impractical due to its inefficiency, considering the time and cost it requires in comparison to small scale modelling. Instead, a small-scale model can be created and subjected to the same stress conditions using a centrifuge for testing (Details mentioned in chapter 3).Also, testing models using a centrifuge helps us to understand the fundamental mechanisms of deformation and failures, and also provide benchmarks that can be used to verify numerical models.

The model instrumentation follows a similar approach as that described in Bienen et al. (2018). Moreover, it is crucial to examine the undrained behavior of dense sand in order to address the research questions. Consequently, two modifications have been implemented: the inclusion of a needle sensor and the utilization of a high viscosity fluid. The primary objective of using a high viscosity fluid with a viscosity of 500 cSt is to closely replicate undrained behavior (Bienen et al. (2018)). To validate this, a sensor capable of measuring pore pressures at the caisson's tip is employed. This measurement aids in determining the

disparity between excess pore pressures at the top and bottom, which indicates whether the behavior is undrained.

Figure 2.10 presents the flow chart showing the research strategy. However, deciding the test loading rates was an iterative process, each test was analysed and further loading rates were decided.

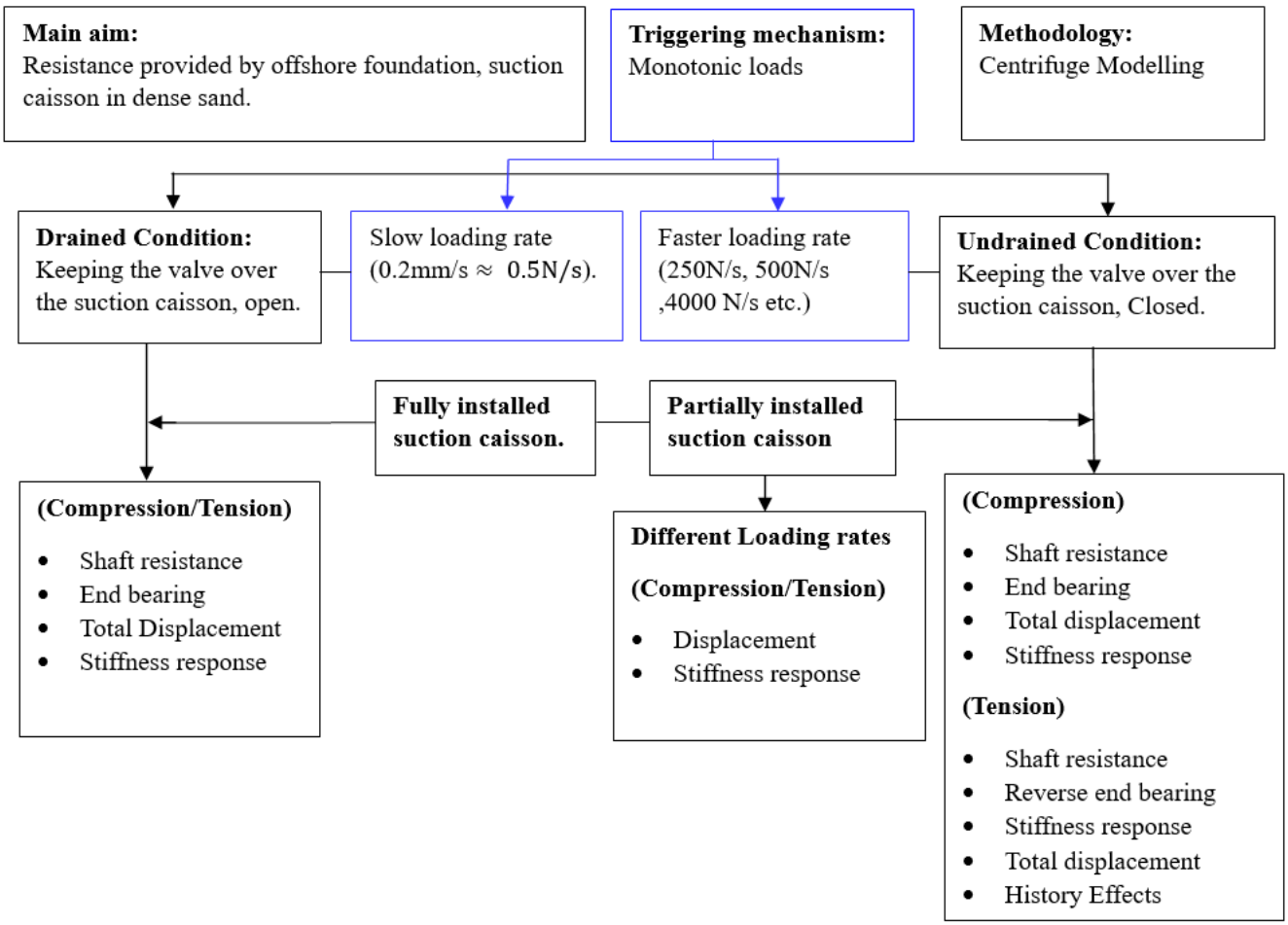

Figure 2.10: Research strategy (Adapted style from Zhang (2020))

Chapter 3

Physical Modeling

This chapter presents a comprehensive overview of the steps involved in conducting centrifuge modeling and provides detailed information about the various components involved and their respective functions. It is important to note that, since the dimensions of the prototype are scaled down to model scale, all dimensions mentioned in this chapter are model scale unless stated otherwise.

3.1 Principles of centrifuge modelling

1. Centrifuge modeling: Centrifuge modeling allows for the reduction of both physical size and time scale while maintaining the similarity of stress and strain conditions. The model is constructed at a reduced scale compared to the prototype, ensuring that the relevant physical phenomena are accurately reproduced.

2. Centrifugal acceleration: The centrifuge generates increased gravitational forces by rotating the model at a high speed. The centrifugal acceleration applied to the model simulates the increased stresses that would be experienced by the prototype under real gravitational conditions.

3. Stress similarity: The aim of centrifuge modeling is to achieve stress similarity between the model and the prototype. By adjusting the rotational speed and model size, the centrifuge creates a stress field in the model that is equivalent to the stress field in the prototype at a reduced scale. The acceleration experienced by soil particles in the centrifuge model is representative of the prototype under gravitational acceleration. This allows for the simulation of soil deformation, stability, and failure mechanisms under realistic conditions.

4. Instrumentation and measurement: Various sensors and instruments are used to monitor and measure the behavior of the model during centrifuge testing. These measurements provide valuable data on factors such as displacements, stresses, pore pressures, and deformations, which help in understanding the geotechnical response.

3.2 UWA geotechnical centrifuge

The different components utilized during a centrifuge experiment are presented below, with each component's function and usage explained in detail. The experimental arrangement is similar to that used in Bienen et al. (2018) and Stapelfeldt et al. (2020) with some additional instrumentation mention in following section.

3.2.1 Beam centrifuge

A 3.6m diameter beam centrifuge is utilized in this project (M. F. Randolph et al. (1991)). The set up includes a beam with sufficient space on one side to hold the sample and a counterweight on the other side to maintain balance. The beam is then rotated at a specified acceleration to generate a field with a higher g-value. The centrifuge used has a capacity of 40 g-tonnes and can spin a 200kg mass with an acceleration of 200g. Its maximum sample dimensions are 1300mm in length and 390mm in width. A two-dimensional actuator is incorporated for the application of various motion conditions, whether load or displacement controlled. Figure 3.1 illustrates the centrifuge utilized for the required experiments.

3.2.2 Strong box

The purpose of the rectangular metal box is to simulate the area of interest in the given problem, and it houses the sample to be analyzed. The box measures 650mm by 390mm in plan, with a height of 325mm, and is situated on one arm of the beam centrifuge, as illustrated in Figure3.2. While aluminium is used to construct the strong box in this particular experiment, glass boxes are often used when PIV (Particle image velocimetry) analyses are required. The dimensions are scaled down by a factor of 1/N, and since the tests were conducted under 100g acceleration, the strong box represents an area of 65m by 39m in prototype scale.

3.2.3 Suction caisson

During the experiments, an 80mm diameter aluminum model caisson with a height of 80mm and top plate thickness of 10mm was used to represent a scaled-down version of an 8m diameter and 8m height prototype under 100g acceleration. The caisson was equipped with two pore pressure transducers, two total pressure transducers, and a digital sensor to measure tip pore pressure (Detailed in section 3.2.1). A needle and digital pore pressure sensor were also used to measure pore pressure at the tip of the model caisson. The caisson was made of anodized aluminum with a skirt roughness of approximately 0.8 micrometer.

3.3 Instrumental cetup

3.3.1 Caisson instrumentation

The model is instrumented to measure different parameters like pore pressures, displacement etc. The instrumentation comprises three pore pressure transducers (PPTs) and

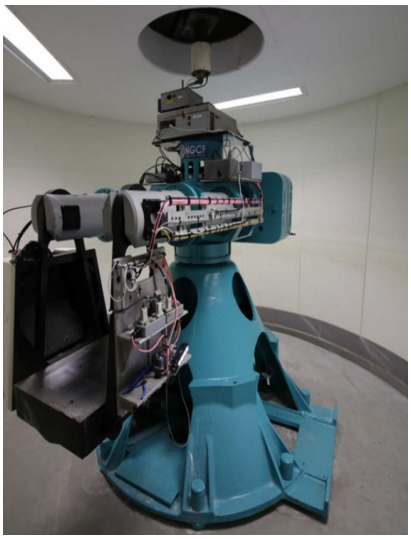

Figure 3.1: Beam Centrifuge

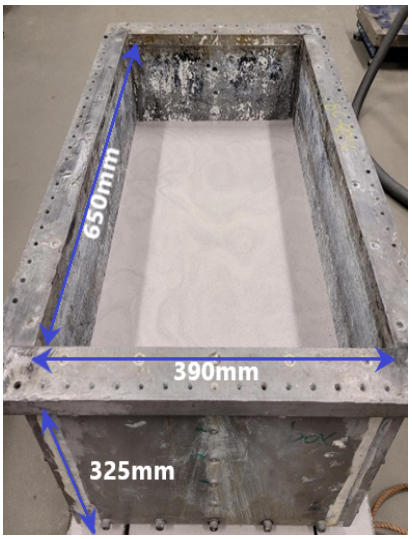

Figure 3.2: Strong box

two total pressure sensors (Top TPT and lid invert TPT). Among the PPTs used, two were Digital PPTs (PPT1, PPTN) that provided a wider range of readings, while one was gel-based (PP T2). One of the digital PPTs was assembled using a metal tube to enable reading of tip pore pressures (as shown in figures 3.3 and 3.4). It is important to note that the needle itself provides some resistance, which needs to be accounted for in calculations. All the sensors were calibrated in a calibration chamber. Although the digital sensors were pre-calibrated, their readings were verified using a digital box. The TPTs and gel based PPT have a capacity of 700kPa, while the digital PPT can measure pressure up to 3 MPa. Additionally, an LVDT (Linear variable displacement transducer) of 20mm length was utilized to determine the displacement of the caisson, which was positioned between a fixed reference beam and the top of the caisson lid .

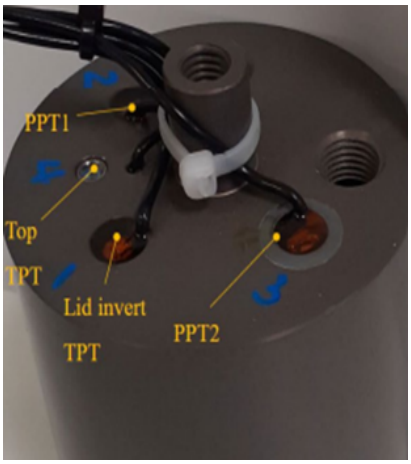

Figure 3.3: Multiple sensors

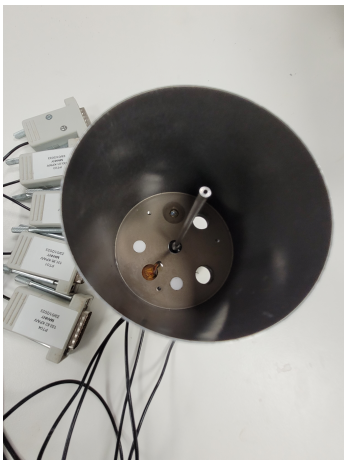

Figure 3.4: Needle sensor

3.3.2 Load application and installation equipments

A syringe pump was used to Install the caisson by use of suction under the high gravity field generated during centrifuge rotation.The pump is connected to a pipe and a 3-way valve that is operated by a motor and wire system, that can be manipulated while the centrifuge is running. The 3-way valve serves three purposes: first, to Connect the caisson to the syringe pump, second, to vent the suction caisson for self-weight installation, and third, to seal the caisson during load application. (Figure 3.5 represents the elaborated version of experimental setup). Another part of assembly is actuator. It is used for application of horizontal or vertical loads or displacement to the suction caisson model. The motion is provided by the servomotors which drive the vertical and horizontal leadscrews. The actuator can achieve a maximum variable speed of $3mm/s$ and a minimum variable speed of $0.002mm/s$. Additionally it is connected to a load cell that has a compression capacity of 7KN and a tension capacity of 5KN.

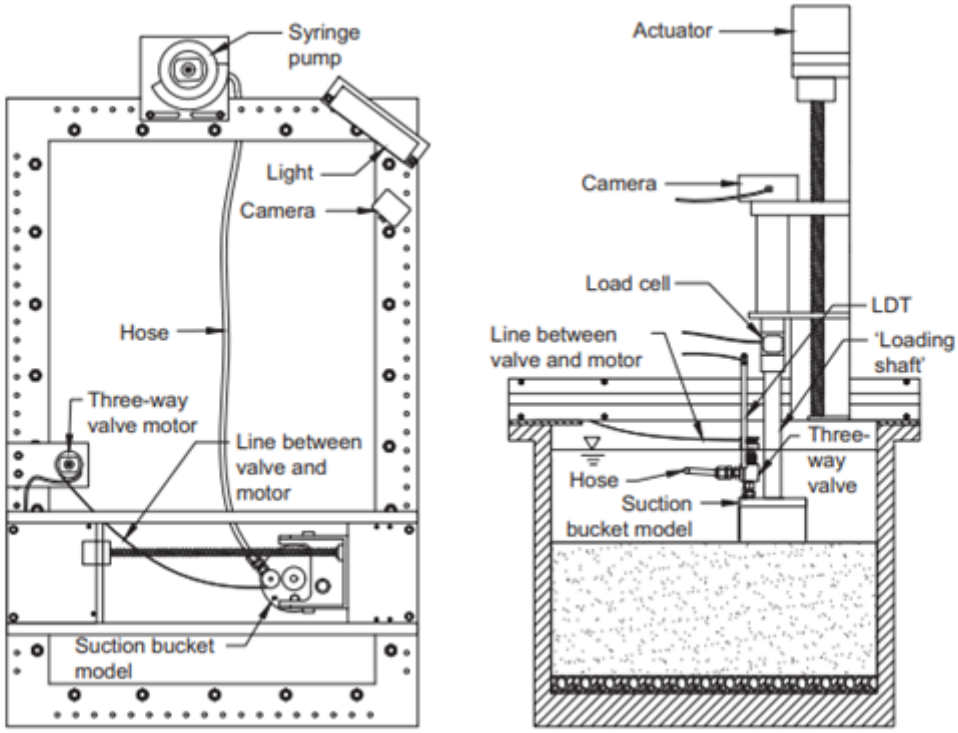

Figure 3.5: Experimental setup (Stapelfeldt et al. (2020))

3.4 Sample preparation

3.4.1 Soil characterisation

To evaluate the characteristics and spatial variability of each sample, cone penetrometer tests (CPTs) were conducted during the flight. These tests involved the use of a 10 mm

diameter model scale cone piezocone penetrometer, which was penetrated at a certain velocity. In Figure 3.6, the red portion in the figure represents the CPT test conducted before testing, while the blue portion represents the CPT conducted after testing. Additionally, the suffixes "a" and "b" are used to distinguish between the two strong boxes.

It can be observed that the top portion of the sample appears slightly disturbed (as expected as its more exposed to the environment forces like the high viscosity fluid), while the region between 40mm and 70mm shows uniformity (which is region of interest). Further examination reveals that the soil remains unchanged up to the experimental depth. However, beyond this depth, there are indications of disturbance. Also, The relative density of both sample range between 75% to 82%.

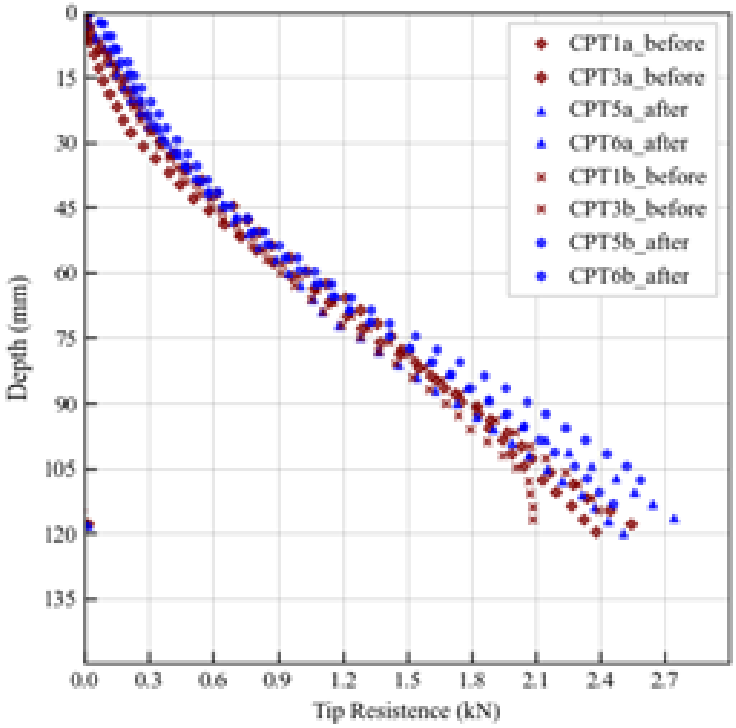

Figure 3.6: CPT results before and after test

3.4.2 Dry sample

UWA SF silica sand was used for the tests, properties of the soil are adopted from previous referred work that use the same sand. The UWA SF silica sand has a specific gravity of 2.67 and minimum and maximum dry densities of $1497 kg/m^3$ and $1774\ kg/m^3$ respectively.(Chow et al. (2019))

The sample was prepared using dry pluviation, It involves the use of compressed air to drop sand particles from a certain drop height (800mm) onto a surface, allowing them to settle and form a dry, uniform layer. In this case a relative density of 70-80% was targeted. The sand was poured into a sand pluviator Figure 3.8, which is essentially a small hopper

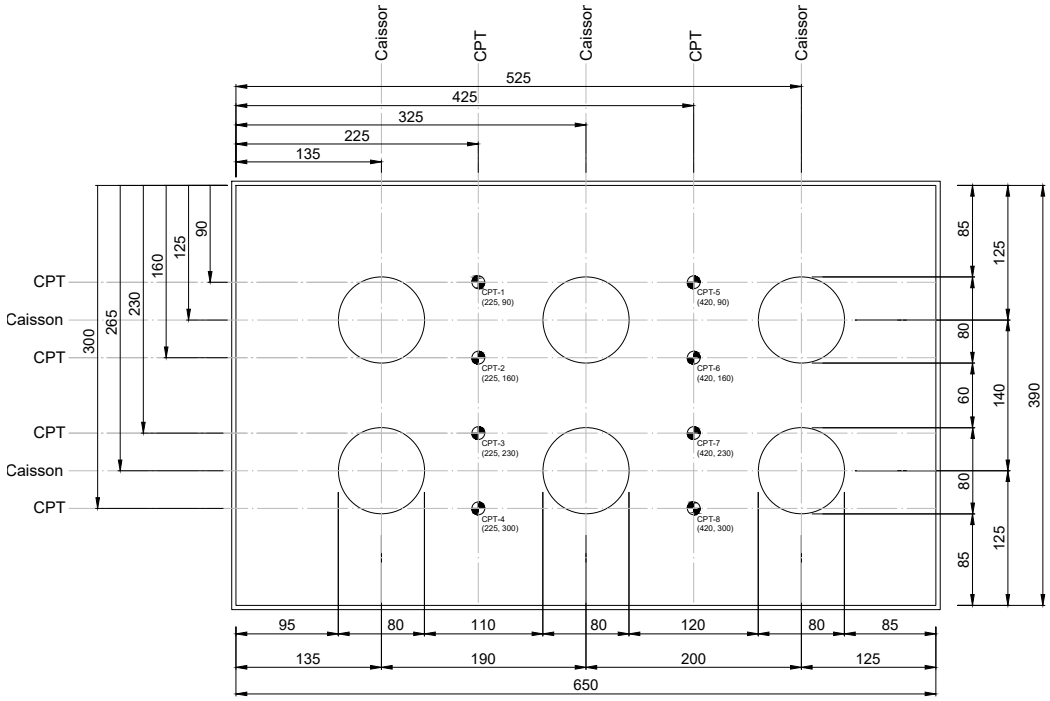

Figure 3.7: Test Layout

with a hole at the bottom. The pluviator was mounted on a stand at a certain height above the surface where the sand layer will be formed. Compressed air was used to force the sand through the hole in the pluviator and out of the bottom. The sand particles drop from the pluviator and form a uniform layer on the surface below. The horizontal velocity($70mm/s$) and the slit size (2mm) was also adjusted to achieve the required relative density. Two such samples of similar relative density were made.

3.4.3 Fluid preparation

In order to replicate the increased gravitational force within the centrifuge, a specific viscosity of pore fluid (referred to as Ng) is selected. This choice ensures that the permeability of the soil, when saturated with this fluid, matches that of the prototype under normal gravity conditions (1g) with water. The adjustment of the fluid viscosity is necessary due to the opposing influences it has on Darcy's coefficient of permeability (k), as explained in various studies such as those conducted by Tan & Scott (1985), Taylor (1987), and Dewoolkar et al. (1999).

The formula for k is expressed as gK/ν, where g represents the gravitational acceleration, K is the intrinsic permeability of the soil, and stands for the kinematic viscosity of the pore fluid. For water, the value of k is approximately 10^-6, 10^{-6} or 1 cSt. However, for the initial five samples, the chosen pore fluid has a viscosity that is 100 times higher than water. Nonetheless, the objective was to achieve behavior similar to undrained conditions,

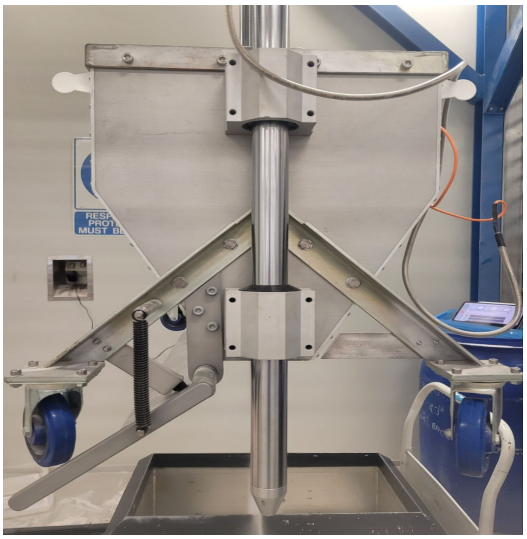

Figure 3.8: Sand pluviator

which led to the selection of a viscosity of 500 cSt.

To create the viscous fluid, methylcellulose was employed at a concentration of 2.27%. The mixture was prepared by combining boiling water with the methylcellulose and then allowed to cool before being used for saturation purposes.

3.4.4 Sample saturation

Sample saturation became tricky due to the high viscosity of the fluid. It was tried to pump at slow rate, however resulted in a piping failure as shown in 3.9(a) . Hence, it was later staurated using the centrifuge, such that higher stress conditions can allow faster rate of pumping (i.e 0.434 ml/s) without any risk of piping. The assembly can be seen in Figure 3.9(b) where a small pump is connected to caisson containing visvcous fluid and the other side of pipe is connect in valve that provides further connection through the center of centrifuge to the sample in flight.

Figure 3.9: Saturating using centrifuge (a) Pipping failure (b) Connection provided to pump fluid

3.5 Scaling principles

In geotechnical centrifuge testing, the terms "model scale" (shown in figure 4.2) and "prototype scale" (shown in figure 4.1) refer to the relationship between the physical model tested in the centrifuge and the real-world prototype it represents. Here are the differences between these two scales:

Model Scale: Model scale refers to the reduced size of the physical model that is tested in the centrifuge. The dimensions of the model are scaled down in proportion to the prototype. The purpose of using a model scale is to replicate the behavior of the prototype under scaled-down conditions, allowing for more practical testing within the limited space and capabilities of the centrifuge.

Prototype Scale: Prototype scale refers to the actual size and dimensions of the geotechnical structure or system being studied. The prototype represents the real-world scenario for which the geotechnical centrifuge testing aims to provide insights and predictions. The results obtained from prototype-scale testing can directly relate to the performance and behavior of the full-scale structure or system.

Hence, Figure 3.10 (Ng (2014)) presents scaling factors to change model scale values to the prototype scale.

Parameter	**Units**	**Scaling Factor (prototype/model)**
Gravity	m / s^2	1/N
Linear dimension	m	N
Volume	m^3	N^3
Stress	N/m^2	1
Force	N	N^2
Strain	Dimensionless	1

Figure 3.10: Centrifuge-scale-factors

In addition to the scaling factors mentioned above , there are other beneficial scaling factors that can be employed to adjust the loading rates. Since the fluid with a very high viscosity was utilized, scaling the time can be employed to achieve the actual-scale load rates. Time and coeff of consolidation scaling factors include 5 because the viscosity of fluid chosen for modelling is 5 times more than the scaled viscosity of water. (detailed explanation in section 3.4.3)

Parameter	**Scaling Factor (prototype/model)**
Coeff of consolidation	5N
Time (Used high viscosity fluid)	N/5

Figure 3.11: Scaling factors for time

3.6 Test procedure

1. Centrifuge start: Reaches level of 100g

2. Sensor check: The caisson was fitted with several sensors, including a new addition of needle sensors. To confirm the functionality of the newly added needle sensors in the caisson, a sensor check was performed. This test was performed in the free fluid over the sand layer. The caisson was subjected to consistent up-and-down movement of approximately 8mm to ensure that the readings provided by the sensors were accurate.

3. Self-Weight Installation: To replicate the self-weight installation process, a load rate of 1 N/s was applied to the caisson until the overall load reached 350N. The selection of this load was based on a conversion from the prototype scale, which accounted for the weight of the caisson and jacket (x). This corresponded to a stress(V/A) of 70KPa and a load of 350 tonnes per caisson at the prototype scale. The load was sustained until the complete dissipation of pore pressure. This step was undertaken to adhere to the field procedure.

4. Suction Installation: The 3-way valve is switched to suction pump in this step, to proceed with suction installation. The suction rate was kept $2mm/s$ and it was continued until the desired depth of L= 70mm was reached. The syringe pump piston advancement rate of 2 mm/s (reflecting a pumping flow rate of 982 mm3/s). The pumping rate was shown to have a negligible effect on the caisson response to loading (Stapelfeldt et al., 2020, where the pumping rate varied from 266.0 mm3/s to 1664.0 mm3/s).

5. Super-structure weight: The assumed case study involves a caisson with a wind turbine installed on top. So, the additional load is applied to the caisson for realizing the site condition. In this case it is calculated to be additional 150N. Hence making the total load of structure to be 500N. This is equivalent to 100 Kpa at prototype scale i.e. 150 tonnes of load.

6. Pre shearing: This step was adopted to stimulate the bedding-in process of the field (Andersen, 2015). Before the high monotonic load rates, the structure must have gone through a cycle of load, this is achieved by performing 400 cycles with an amplitude of 6kpa (30N) before applying the final load.

7. Monotonic load: The choice of monotonic loading method was based on the objective of the test, resulting in varying rates and techniques used in each test. Each load was reduced to mean load after reaching maximum point. This was done as gives more relevance with field conditions. Also, all loads were uniformly increased at a constant rate.

8. Extraction: Once the monotonic loading had concluded, the load was returned to the mean level of 500N and then the caisson was extracted. In case of monotonic compressive loading the extraction was performed at different rates. The purpose of this was to conduct a preliminary analysis for monotonic tensile loading, and the extraction rates were determined based on the goals of the test.

9. Post sensor check: In order to verify the effectiveness of the needle sensors, the procedure from step 1 was repeated. However, it was discovered that in some instances the needle sensors had been disrupted by sand infiltration.

3.6.1 Installation

Caisson Installation was done in flight, in two steps. First, the Self-weight installation and than the Suction Installation. In order to simulate the self-weight installation process, the self-weight of a typical caisson connected to a jacket foundation was calculated to determine the applied load which was equivalent to 350N in model scale. Hence, a load rate of 1 N/s was gradually applied to the caisson The loading continued until the total load reached 350N, corresponding to a stress of $70kPa$. This load was sustained until the pore pressure completely dissipated, following the same procedure as in the field (Kay et al. (2021)). To perform suction installation the valve was switched towards the syringe pump. The suction rate was kept $2mm/s$ and it was continued until the desired depth of L= 70mm was reached. Same procedure was followed for both, fully installed and partially installed suction caisson.

Figures 3.12a and 3.12b shows fully installed caissons, indicating that they shared the same requirement for an embedded depth of 70mm establishing contact with the sand surface. This assertion can be confidently made due to the presence of a metal plate affixed to the caisson prior to installation, required to ensure complete contact. The graphs portray the actual depth on the y-axis, excess pore pressure on the bottom x-axis, and vertical stress on the top x-axis. As the installation process employs suction to induce vertical stress, the excess pore pressures are depicted as negative values.

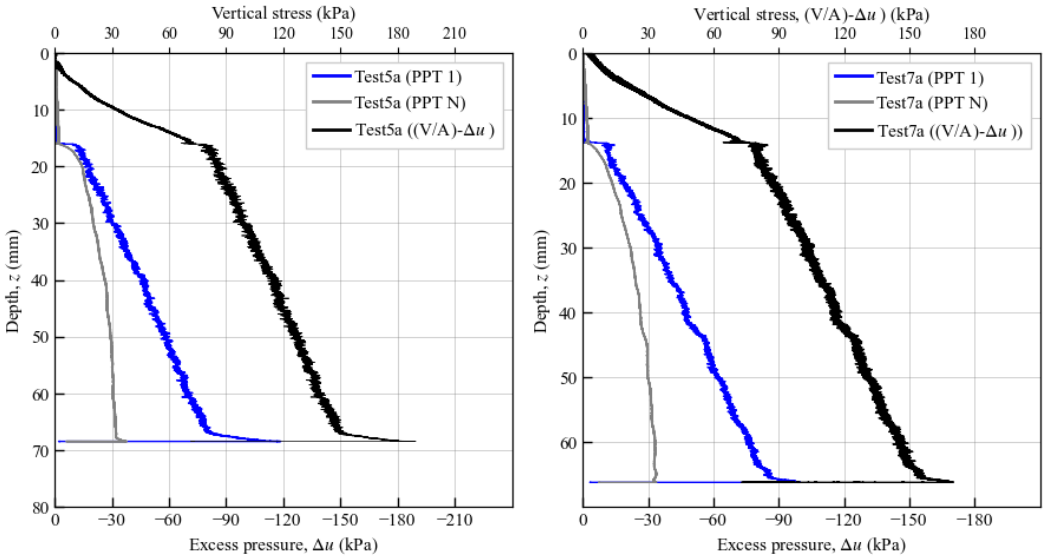

Figure 3.12: a) Fully Installed caisson test1a b) Fully Installed caisson test7a

It is evident from both Figures 3.12a and 3.12b that a change in slope occurs in the

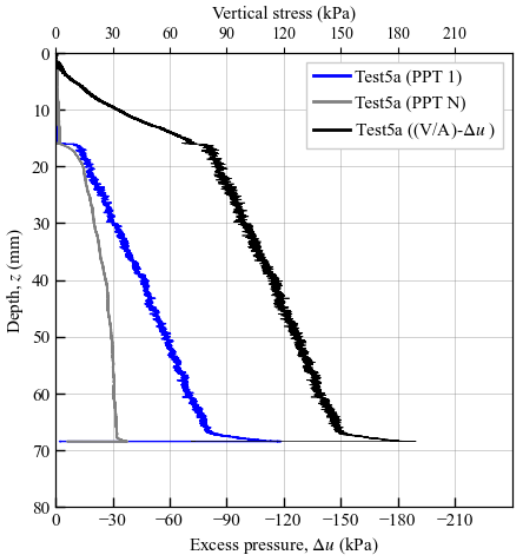

Figure 3.13: Partially Installed caisson test5a

excess pore pressure and vertical stress curves before reaching the desired embedment depth that is required to develop full contact with the sand surface. This suggests the possibility of plug heave. By calculating the difference between the observed depth at which the slope change occurred and the desired embedded depth, the magnitude of plug heave can be determined.

Hence fully installed caissons showed a plug heave of 2% to 5% (as shown in Figure 4.15) due to suction installation. Nevertheless, this is not perceived to influence the shaft resistance of fully installed caissons. A similar level of suction is also applied in partially installed caissons, then it's assumed that a similar plug developed can occur (no instrumentation could confirm this directly). All the above arguments are also valid as per Tran et al. (2004).

3.6.2 Test matrix

Two sets of tests were carried out in two strong boxes. The first set of tests, represented in Table 3.1 and Figure 3.14, involved compression loading followed by tension loading. In contrast, the second set of tests, shown in Table 3.2 and Figure 3.15, consisted of only tension loading without any prior significant compression history.

The figure 3.14 and figure 3.15 illustrates that the test involved initial stages, which are clearly depicted in by labeling. Both tests were carried out at a constant displacement rate of $0.002mm/s$. It is crucial to note that "FI" refers to the fully installed caisson and "PI" represents the partially installed caisson. Also, subsequent meanings of partially installed and fully installed caisson can be understood by referring to Figure 4.2 . Referring to Figure 3.14, the graph displays the relationship between vertical load (y-axis) and time in seconds (x-axis). It illustrates the testing sequence conducted in strongbox A, where two consecutive tests were performed. Once the centrifuge reached a 100g level, self-weight and

	COMPRESSION								TENSION							
Test ID	1a	2a	3a	4a	5a	6a	7a	8a	1b	2b	3b	4b	5b	6b	7b	8b
Valve	Open	Closed	Closed	Closed	Open	Closed	Closed	Closed	Open	Closed	Closed	Closed	Closed	Open	Closed	Open
Gap	Yes	Yes	Yes	Yes	No	Yes	No	Yes	No	Yes	Yes	Yes	No	Yes	No	Yes
Loading rate	0.002 mm/s	3mm/s	500N/s	2000 N/s	0.002 mm/s	4000 N/s	4000 N/s	4000 N/s	0.002 mm/s	3mm/s	3mm/s	500N/s	250N/s	0.002 mm/s	50N/s	0.002 mm/s
Zo(mm)	73.6	68.8	70.4	68.9	68.8	70.0	66.2	69.7	79.1	73.1	73.4	71.1	70.9	71.8	68.0	71.82
Zf(mm)	79.1	73.1	73.4	71.1	70.9	71.8	68.0	71.82	-	-	-	-	-	-	-	-

Table 3.1: Monotonic Compression followed by Tension loading

	TENSION					
Test ID	1c	2c	3c	4c	5c	6c
Valve	Open	Closed	Closed	Open	Open	Open
Gap	Yes	Yes	Yes	Yes	No	No
Loading rate	0.002 mm/s	3mm/s	50N/s	10N/s	0.002 mm/s	0.002 mm/s
Zo(mm)	67.66	69.87	70.18	68.78	66.51	66.66
Zf(mm)	-	-	-	-	-	-

Table 3.2: Monotonic Tension loading.

suction installation were carried out. Following this, pre-shearing was applied until pore pressures stabilized. Monotonic compression was then applied up to $7kN$ and subsequently unloaded to 500N. Tensile loading was applied until failure. In the graph, compression is represented by the blue line, while tension is depicted by the red line.

Moving on to Figure 3.15, it also presents the relationship between vertical load (y-axis) and time in seconds (x-axis). This graph demonstrates the testing procedure employed in strongbox B. The initial steps followed the same protocol as in strongbox A until the pre-shearing stage. Subsequently, tension load was directly applied until failure.

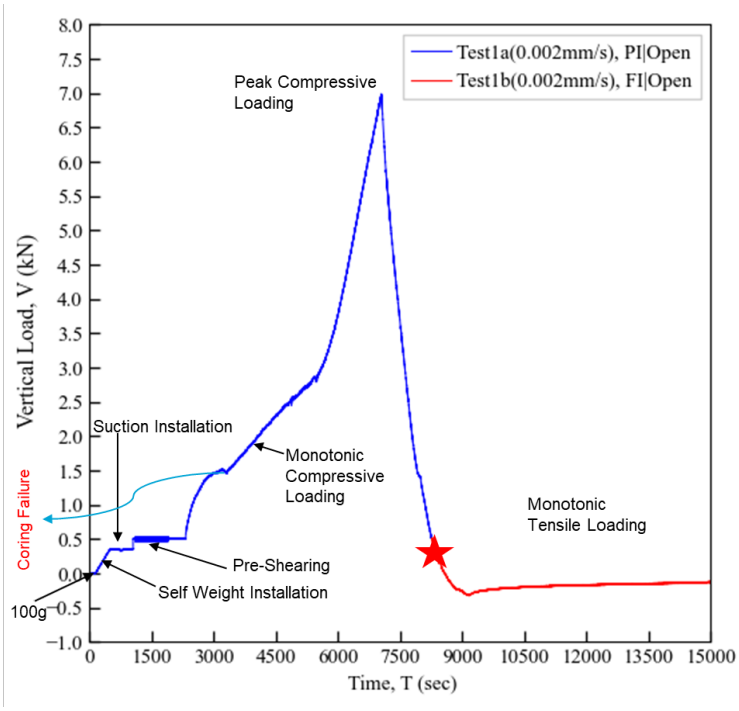

Figure 3.14: Compression followed by Tension loading

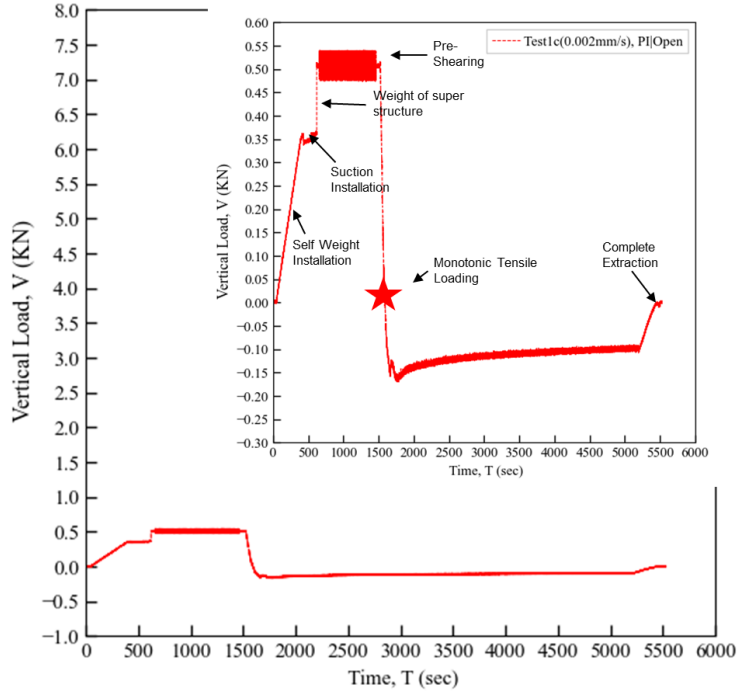

Figure 3.15: Tension loading without compressive loading history

Chapter 4

Results and discussions

This chapter presents all the experimental results obtained from the centrifuge test. All the results aim to answer the research questions outlined in section 2.7 . The chapter begins with some additional findings done for installation process, which was not directly aimed in the research question. Rest of the chapter is organised as follows.

In section 4.1 a representation of model is shown and the terminologies used throughout the chapter are discussed, to make the interpretation easier for the reader.

In Section 4.2 The results answering the first research question are shown. Where a comparative study is provided between fully installed and partially Installed suction caisson. It aims to provide an idea about how under base filling can or cannot affect the mobilised resistance under different loading conditions.

In section 4.3 The results answering the second research question, regarding the effects of load rate on partially installed suction caisson. Here comparison of different load rates is done for compression and Tension loading conditions, to understand how the resistance is mobilised under different load rates.

4.1 Terminologies

Figure 4.1 and Figure 4.2 shows the equivalent prototype of the tested models. The dimensions are adjusted according to the 100g gravity applied and following the scaling principles showed in figure 3.10.

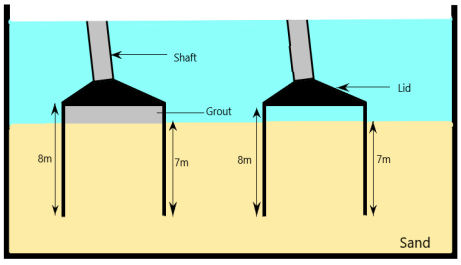

Figure 4.1: Prototype scale

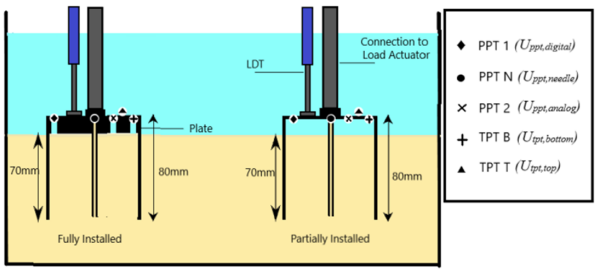

Figure 4.2: Model scale

It is important to highlight a significant aspect concerning the prototype where the under-base filling is simulated in the model using a metal plate. The utilization of a metal plate distinguishes the caisson configurations, where the caisson with the metal plate is referred to as the fully installed caisson, and the caisson without the metal plate is denoted as the partially installed caisson. Moreover, it is noteworthy that, regardless of the assigned names, efforts were made to maintain a similar embedded depth for both caisson configurations.

It is worth mentioning that the process of determining the caisson depth involved manual control, which introduces the possibility of human error. However, any such errors were identified and rectified during the post processing of the results.

Each caisson is equipped with a valve at the top, as described in section 3.2.2. Depending on the test requirements, this valve was either kept opened or closed. However, in field conditions, the valve is typically kept closed once the caisson is installed. Additionally, it is important to note that all compression tests were limited by the capacity of the load cell, maximum load cell available was 7kN, which means that the full compression resistance was not mobilized in any of the tests.

Furthermore, Figure 4.2 shows how the sensors on the caisson were named. This naming scheme is used consistently when sharing the results. The legend that accompanies each graph uses the terms specified in the figure, making it easier to identify and understand the information presented in the analysis.

4.2 Installation effects

Experiments were conducted to assess the performance of partially and fully installed caissons under monotonic compression and tension loading. In one scenario, a valve was deliberately left open to replicate a scenario similar to drained conditions, while in the other scenario, the valve was kept close.

4.2.1 Compression

Figure 4.3 depicts four tests, two with the valve open and two with valve closed. The x-axis represents Excess pore pressures at the top, while the vertical force is displayed on the y-axis. In figure 4.3a, the relative depth is shown, indicating the displacement required to achieve a specific resistance. Figure 4.3b illustrates the total depth, providing insight into the difference in embedded depth.

These graphs feature three variables, as indicated in the legends: the loading rate, whether the caisson is partially installed (PI) or fully installed (FI), and the valve opening. The solid lines in the graphs compare the FI and PI caissons when the valve is kept open and a slow displacement/load rate is applied. Conversely, the dashed lines compare the FI and PI caissons when the valve is kept closed and a high displacement/load rate is applied.

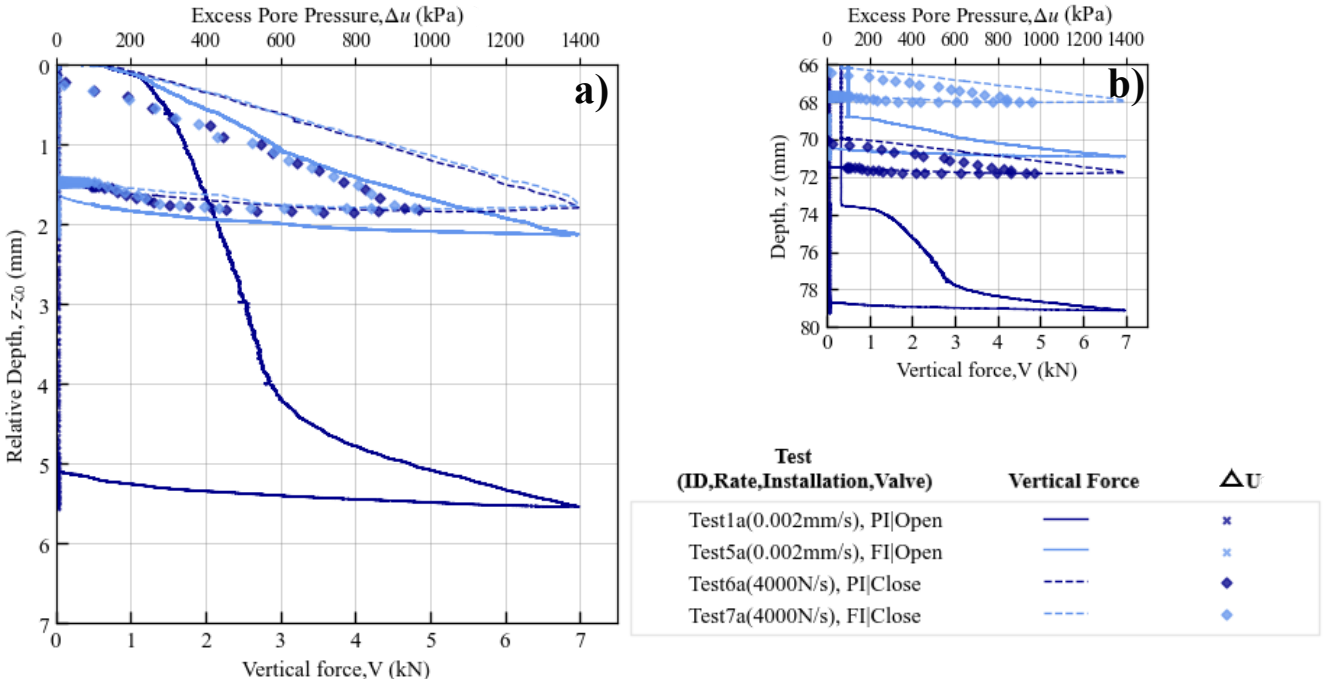

Figure 4.3: Installation effect variation under compression a) with relative depth, b)with depth

When examining Test1a and Test5a, it is observed that the excess pore pressures($U\Delta$) remain nearly zero throughout the test, indicating a closed to drained response (which was the primary objective of keeping the valve open). The vertical force for both the partially installed (PI) and fully installed (FI) caissons overlaps until reaching approximately 1.2kN. Subsequently, the fully installed caisson exhibits a stiffer response compared to the partially installed caisson until approximately 2.7kN. Beyond that point, both caissons demonstrate a similar slope until reaching the load cell limit of 7kN, after which the caisson was unloaded to 500N. Furthermore, the total displacement for the partially installed caisson is approximately 5.5mm, whereas for the fully installed caisson, it is only 2mm.

Based on the above description, it can be inferred that initially, the primary source of resistance for both the partially installed (PI) and fully installed (FI) caissons is the shaft resistance. This explains why the vertical force lines overlap. However, as the test progresses, the PI caisson needs to mobilize the end-bearing resistance, due to its lack of contact with the sand surface, it requires more displacement to achieve the same resistance as the FI caisson, which is already in contact with the sand surface. Therefore, it can be concluded that under drained conditions, both the PI and FI caissons mobilise same shaft resistance (Shown in Figure 4.4). However, the partially installed suction caisson requires more displacement to mobilize the end bearing when compared to the fully installed caisson.

Similarly, when examining the graphs with the valve closed, namely test 6a and test 7a, it can be observed that the vertical force for both fully installed and partially installed caissons overlap throughout the test. Additionally, the excess pore pressure ($U\Delta$) generated remains

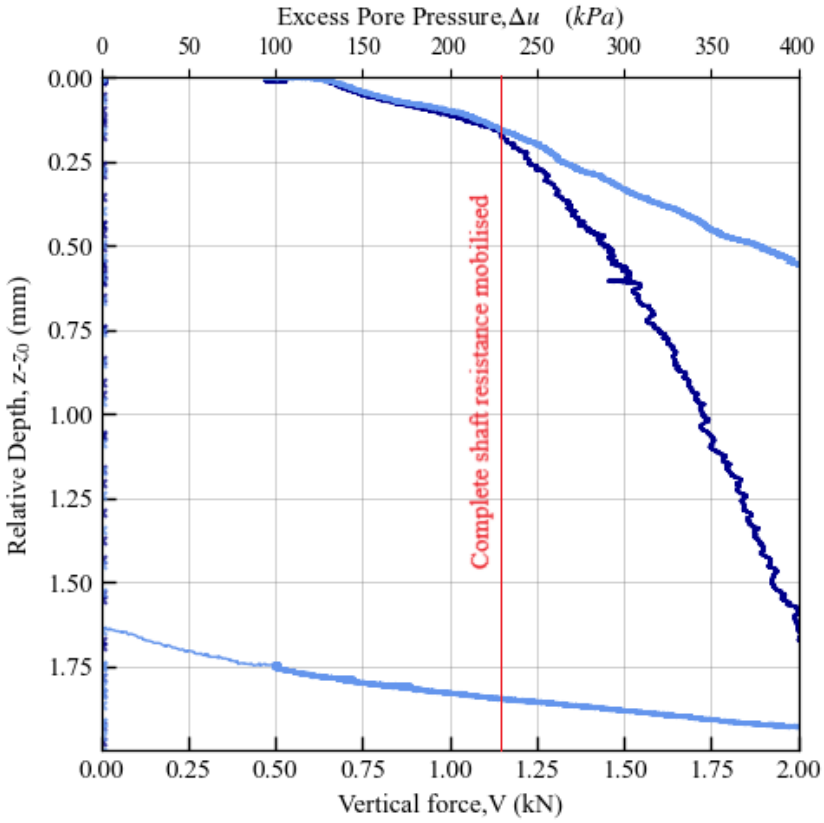

Figure 4.4: Shaft Resistance

consistent in both cases. Furthermore, a total displacement of approximately 1.8mm can be observed in both cases. Therefore, it can be deduced that when the valve is closed and a substantial loading rate is applied, excess pore pressures are generated regardless of the lid contact, resulting in the development end bearing resistance. Although full end bearing could not be mobilized, it is inconclusive whether both caissons will exhibit the same relationship throughout. However, it can be concluded that the presence of a water plug does not hinder the generation of pore pressures, and a close to undrained response can ensure the same capacity in the case of a partially installed (PI) caisson as that provided by a fully installed (FI) caisson. The findings align with the assumptions outlined in the literature review.

4.2.2 Tension

Figure 4.5 presents a similar axis distribution as described in section 4.2.2, but in this case, tensile loading was applied instead of compression. The tensile force is represented with a negative sign, increasing from right to left. As before, the solid lines represent the comparison between fully installed (FI) and partially installed (PI) caissons when the valve is kept open, and a slow displacement/load rate is applied. Conversely, the dashed lines compare the FI and PI caissons when the valve is kept closed, and a high displacement or

load rate is applied.

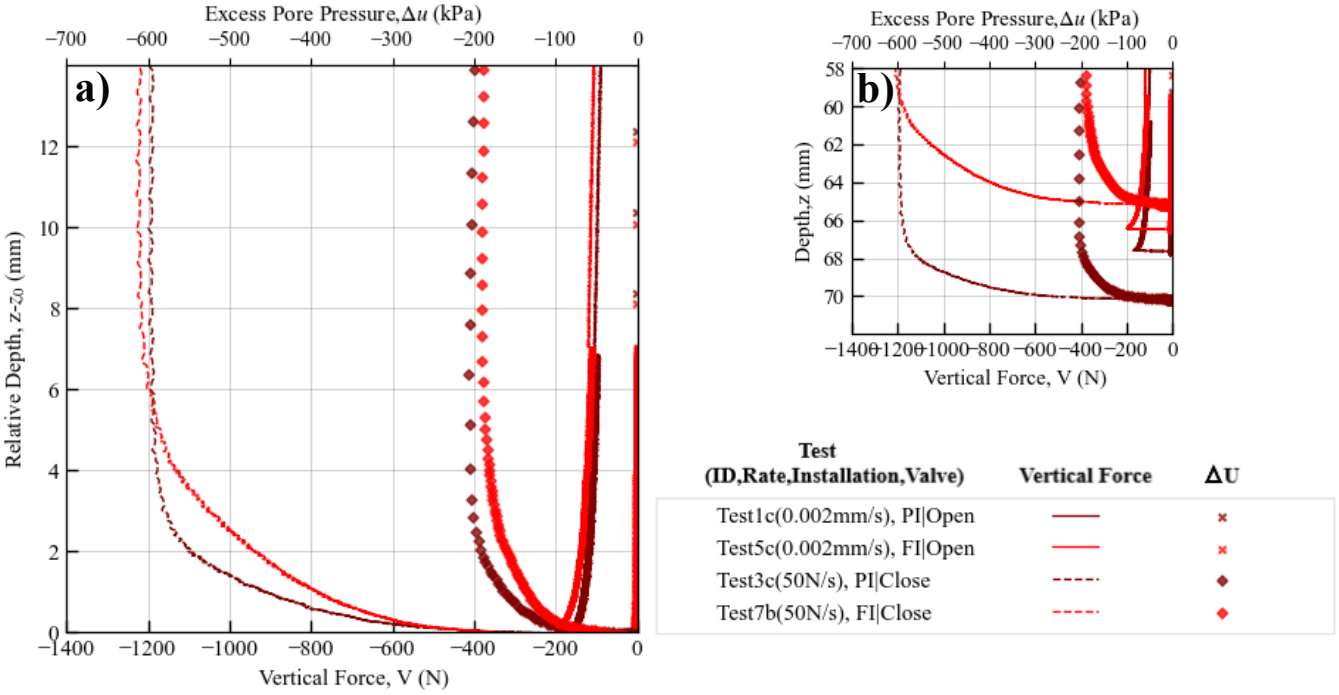

Figure 4.5: Installation effect variation under Tension a) with relative depth, b)with depth

Analyzing the case with an open valve and a slow loading rate, it is observed that both vertical force graphs overlap, and the excess pore pressures remain almost zero throughout the test. This response was expected since, under drained conditions, only shaft resistance is mobilized against tensile loading. Figure 4.5b illustrates that the embedded depth is the same in both cases, resulting in the same shaft resistance. Hence, regardless of installation both cases provide same resistance. It should be noted that slight suction jumps, of about 10kPa were observed in test 5c (open valve), but their magnitude is considered negligible.

Examining test 3c and test 7b, it can be observed that the vertical force lines almost overlap throughout the tests. A slight difference in stiffness response can be attributed to the relative densities of the separate boxes used in each test, as shown by comparing test 6b and 8b (Figure 6.1 in Appendix).

From the comparison between tests 3c and 7b , it can be concluded that reverse end bearing develops after mobilization of shaft resistance. Interestingly, the magnitude of reverse end bearing is nearly six times that of the shaft resistance. Furthermore, it is not affected by the presence of a water plug, as evidenced by the consistent response of both the PI and FI caissons, which is contrasting to the speculation made by Mana et al. (2013)

4.2.3 Load transfer mechanism

Figure 4.7 illustrates the comparison of load transfer under compression loading for both the partially installed (PI) and fully installed (FI) caissons. In the case of a closed valve, it

is assumed that the resistance comprises three components: shaft resistance, tip resistance, and end bearing. To determine the load transfer mechanism, the resistance developed by excess pore pressure is subtracted from the total mobilized resistance, resulting in the calculation of shaft and tip resistance. Similarly, in the case of an open valve, only shaft and tip resistance are considered since the end bearing is not mobilized until 1.5kN. Analyzing tests 1a and 5a, it is evident that till the shaft resistance is completely mobilised, and both the FI and PI caissons exhibit complete overlap. Beyond this point, excess pore pressures are mobilized, which can be observed overlapping throughout the tests. Notably, coring failure occurs earlier in tests 1a and 5a compared to tests 6a and 7a, which is expected as tests 1a and 5a demonstrate a nearly undrained response, potentially leading to a reduction in internal shaft resistance.

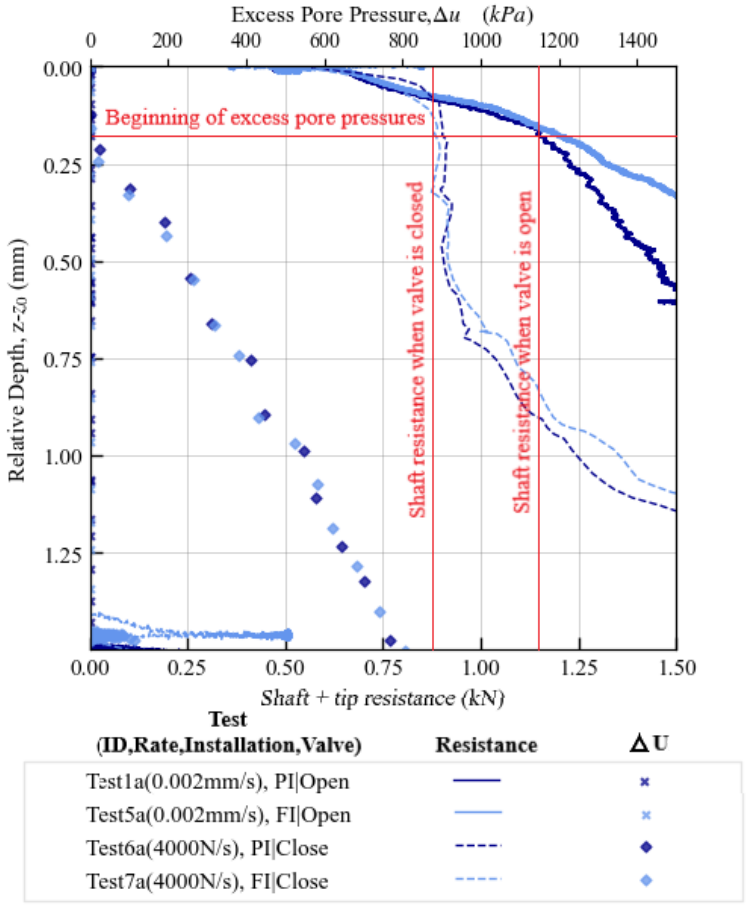

Figure 4.6: Distribution of load

From these observations, it can be concluded that the load transfer mechanism remains the same regardless of whether the caisson is fully or partially installed. The same conclusion can be drawn for tension loading when examining Figure 4.5. Assuming that the main components of resistance are shaft resistance and reverse end bearing, both the PI and FI caissons mobilize shaft resistance first, followed by the reverse end bearing.

4.3 Load rate effects

This section main variable looked upon the load rate and corresponding mobilised resistance for partially or fully installed suction caissons. Here the focus is kept to understand the partially installed suction caisson hence, no comparison is made with fully installed caisson. Also, the valve is kept closed in all cases.

4.3.1 Compression

Figure 4.7 illustrates a comparison of various loading rates for monotonic compression load. It is evident that all loading rates can achieve a resistance of 7kN, but the displacement required to reach this value varies. Specifically, as the loading rate decreases, a higher displacement is needed to mobilize the 7kN resistance. The graph also demonstrates that the excess pore pressure development occurs almost simultaneously for all loading rates, while the dissipation of these pressures is faster for lower loading rates.

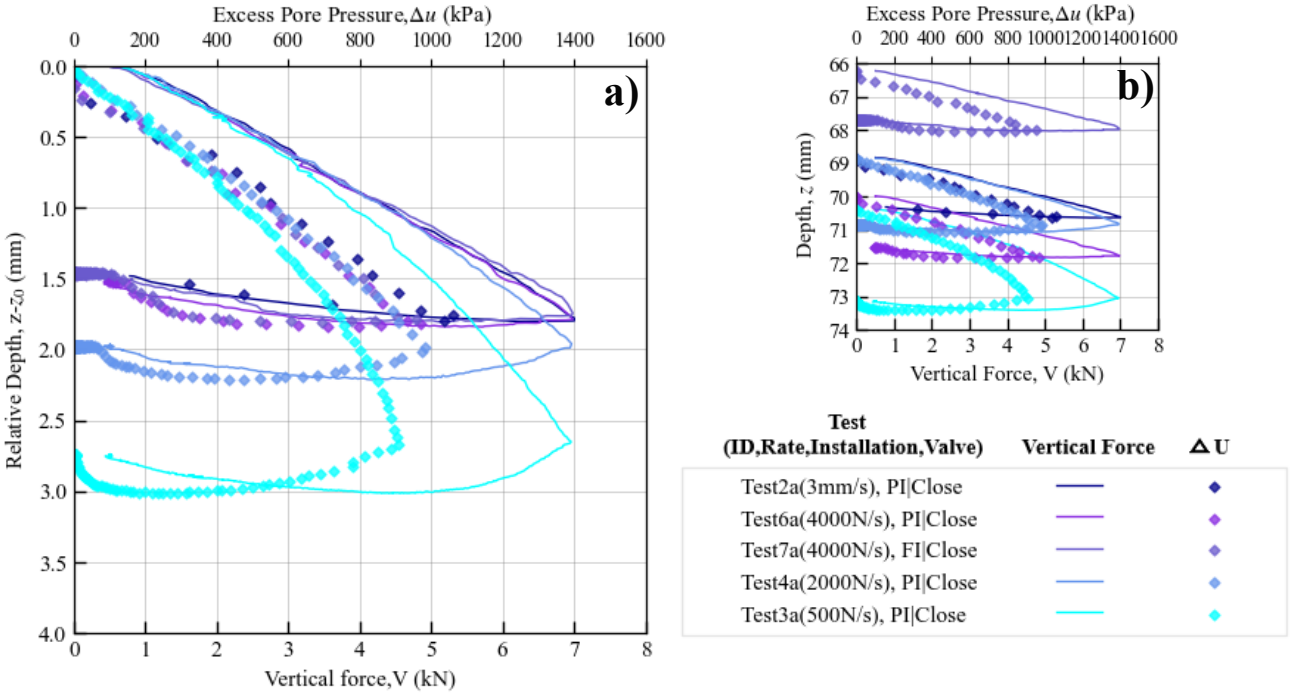

Figure 4.7: Compression Load rate effect a) with relative depth, b)with depth

Hence, a higher load rate leads to a stiffer response compared to a lower load rate, suggesting that greater resistance can be activated with increased the load rate. It is noteworthy that the disparity in load rates between test 3a and test 6a is eight-fold, whereas the variance in their stiffness response is only twofold (as depicted in Figure 4.8), indicating a nonlinear correlation between mobilized resistance and load rate (Dashed line in Figure 4.8) .

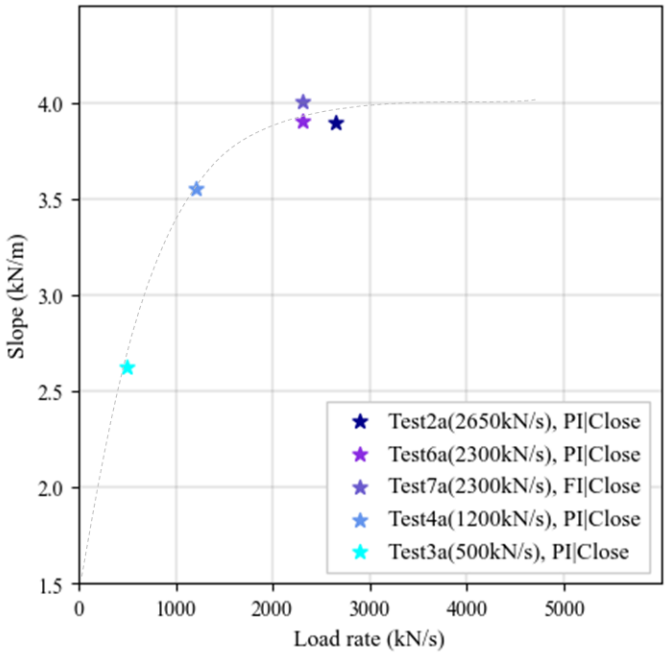

Figure 4.8: Nonlinear correlation between mobilized resistance and load rate

One can make the assumption that the overall resistance consists of three elements: shaft resistance, tip resistance, and resistance mobilised by excess pore pressures (This components was measured using pore pressure sensor at top and multiplied by top plate area to get the value of resistance).Consequently, Figure 4.9a is generated by subtracting the excess pore pressure resistance from the total mobilized resistance and plotting it against relative depth. On the other hand, Figure 4.9b exclusively illustrates the resistance mobilized by excess pore pressure, plotted against relative depth.

Observing Figure 4.9a, it can be seen that the combined resistance provided by the shaft and tip is higher for a lower load rate. In Figure 4.9b, there is an indication of increased dissipation of pore pressures as the load rate decreases. This suggests that the rate of dissipation for excess pore pressures is higher when the load rate is low. As a result, it can be inferred that in such cases, the resistance provided by the shaft and tip will be greater.

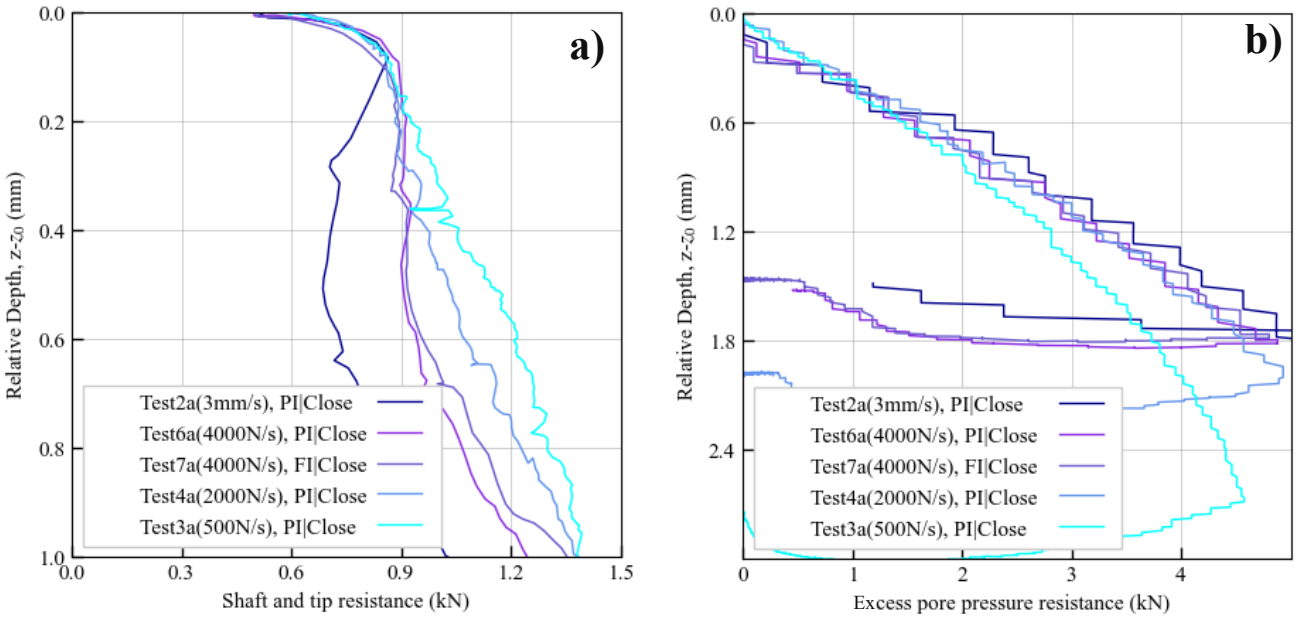

Figure 4.9: Components of resistance a) Shaft and Tip, b) End bearing

4.3.2 Tension

Due to the limitation of cavitation, all the tension tests performed with a closed valve were constrained by this factor, making it difficult to observe the effects of load rate. (cavitation was observed at 200 kPa as seen in figure 4.10a)

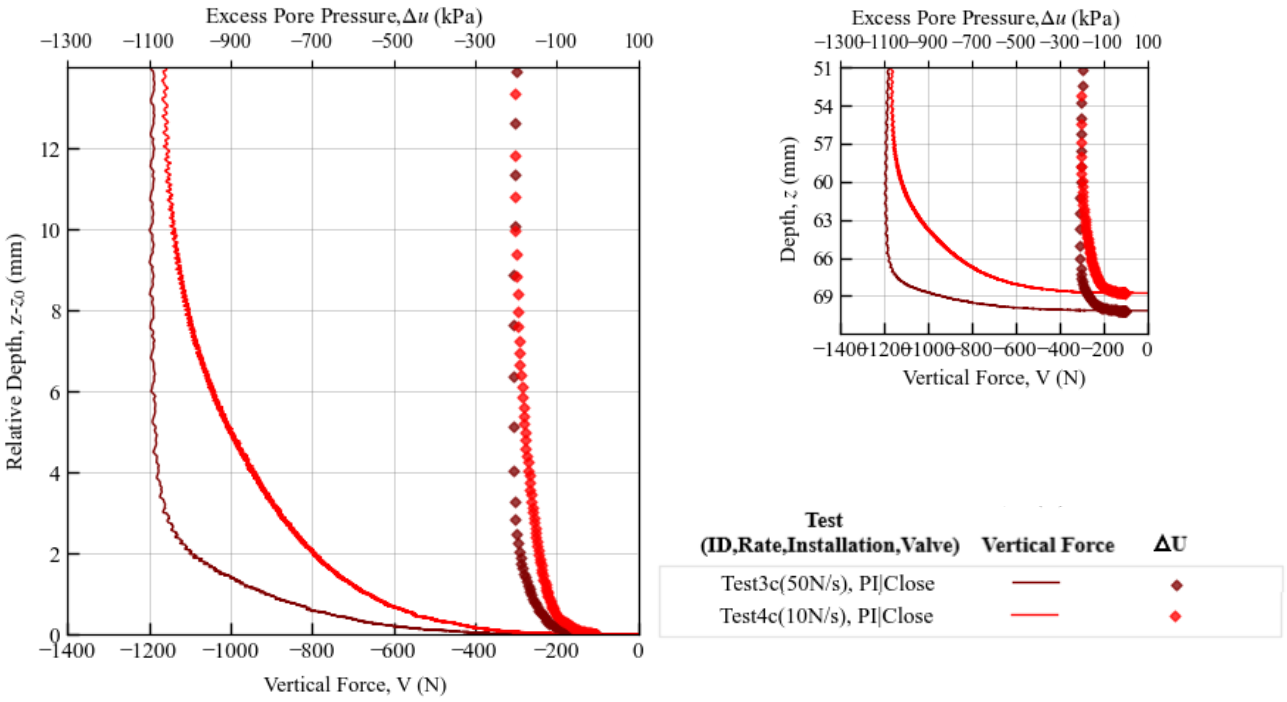

Figure 4.10: Tension Load rate effect a) with relative depth, b)with depth

Consequently, very low load rates were selected to enable the differentiation and observation of the development of reverse end bearing from other load rates. Figure 4.10 depicts the results of test 3c and 4c conducted at loading rates of $50N/s$ and $10N/s$ respectively. Moreover, the embedded depth was kept nearly identical in both cases (as shown in Figure 4.10b). Upon analyzing these figures, it becomes apparent that the higher loading rate exhibits a stiffer response. An interesting observation is that even a slow loading rate of $10N/s$ can still mobilize a significant amount of reverse end bearing (even though at a slower rate than 50 N/s but its extent is also limited by cavitation (at $200kPa$).

4.4 Additional observations

Through the performance of numerous tests aimed at addressing the chosen research question, a wealth of additional valuable information was gathered from the results. The subsequent section elucidates the observed history effect on tension resistance and the noticeable plug heave encountered during installation. It is worth noting that the installation process was carried out (in flight) in a manner consistent with real-world site conditions

and adhering to applicable regulations. Therefore, the data obtained from the installation outcomes proves to be beneficial as well.

4.4.1 History effects

Figure 4.11 provides a comparison among three tests that share the same loading rate and valve opening but differ in their loading history. test 8b involved a monotonic compressive loading at a rate of $4000N/s$ followed by a monotonic tension loading at a rate of $0.002mm/s$. Conversely, test 1c and 5c did not undergo prior compression loading. Figure 4.11 clearly indicates that the stiffness response is consistent across all represented curves. However, the resistance mobilized in test 8b is significantly greater than the other two cases. By examining Figure 4.11b, one can infer that the disparity may be attributed to the embedded depth. Consequently, the vertical load was normalized by the effective vertical force and shaft area to derive a resistance response independent of the embedded depth. The following equation represents the normalization employed:

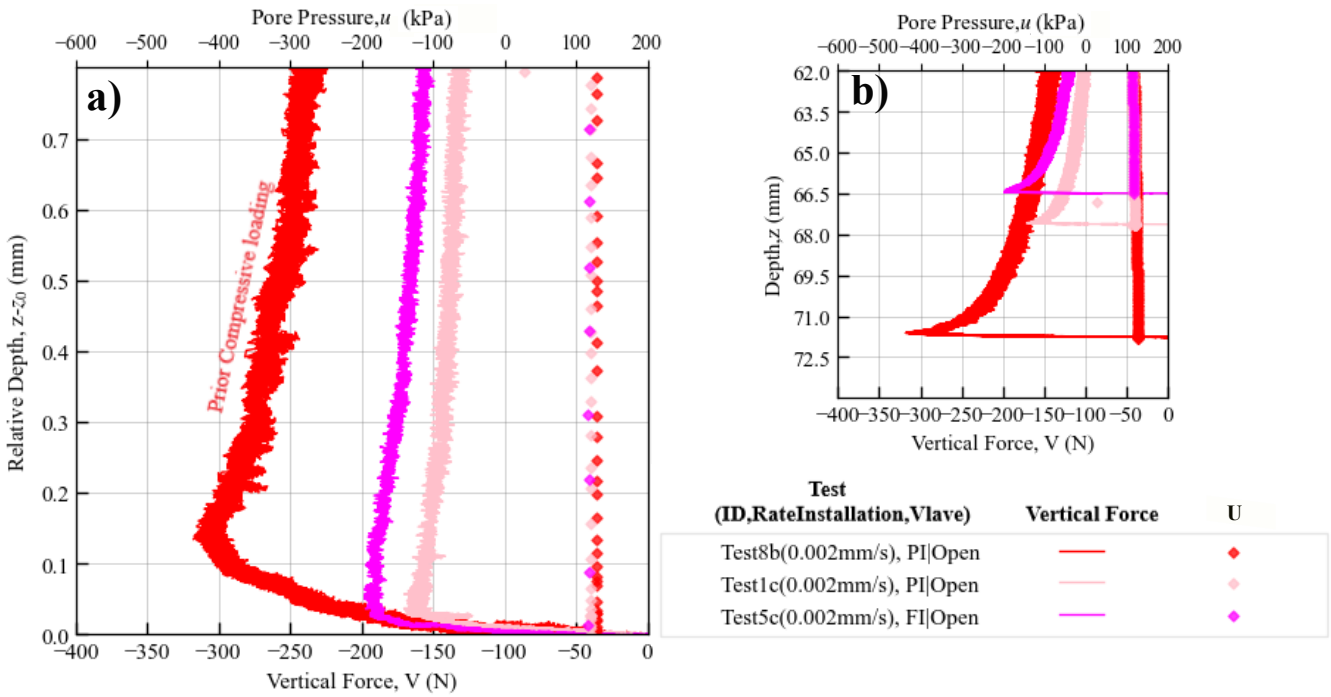

Figure 4.11: Tension with compression history a) with relative depth, b)with depth

$$Q_f = k \tan \delta \sigma'_v A_{shaft} \tag{4.1}$$

$$\frac{Q_f}{\sigma'_v A_{shaft}} = k \tan \delta \tag{4.2}$$

Upon examining Figure 4.12, it becomes evident that the increase in resistance is not attributed to variations in embedded depth but rather to the prior compression loading.

This effect nearly doubles the resistance without displaying any noticeable disparities in pore water pressures. Consequently, it can be inferred that the introduction of a pre-compression stage leads to greater displacements and higher force peaks. Moreover, the difference in peak force between test1c and test5c can be attributed to the slight suction that occurs during peak force (approximately 50kPa), leading to an additional resistance against tension. This phenomenon is evident in Figure 6.3 in the Appendix, where the pressure drop is clearly noticeable in test 5c but not in test 1c.

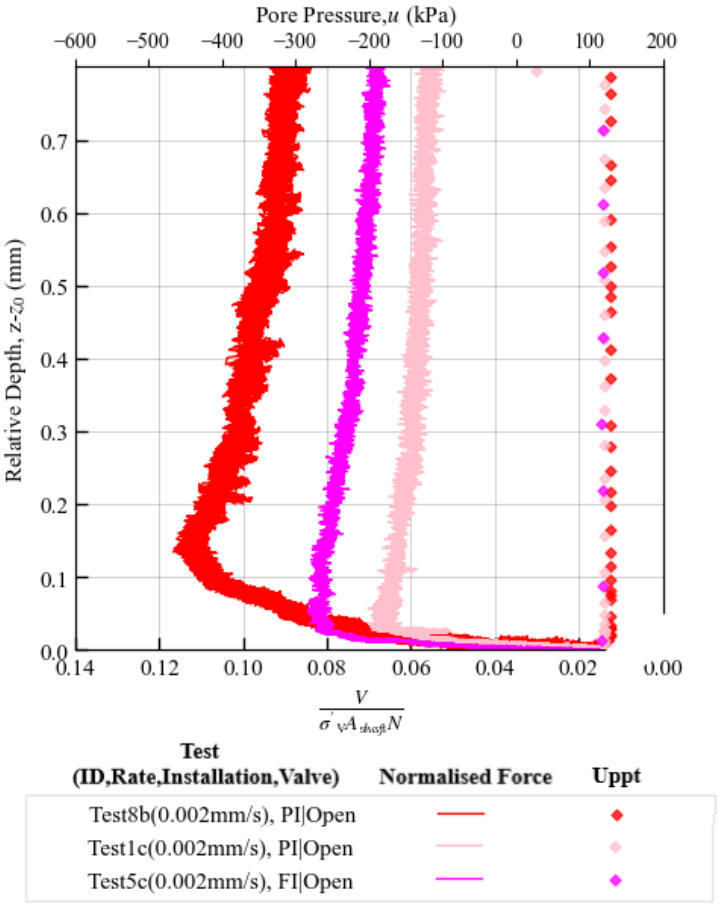

Figure 4.12: Normalized Vertical Force

In order to delve deeper into the history effect on tension resistance, two tests were compared, both employing the same tension loading rate but differing in their compressive loading rate history. Illustrated in Figure 4.13, test 1b and 6b feature an identical tension loading rate and both possess a compressive history. However, the discrepancy lies in the fact that test 1b underwent prior compression at a rate of $4000N/s$ while test 6b experienced a compressive displacement of 0.002 mm/s, equivalent to approximately $1N/s$. It is worth noting that these tests also have different embedded depths, as depicted in Figure 4.13b.A distinction in resistance is noticeable when prior compressive loading was applied at a higher rate. To ensure that this discrepancy is not influenced by variations in embedded depth, a

normalization process was conducted, as described in Equation 4.1. Figure 4.14 illustrates that both graphs overlap, indicating that the disparity in resistance is attributed to the variation in embedded depth rather than the difference in compression loading rate.

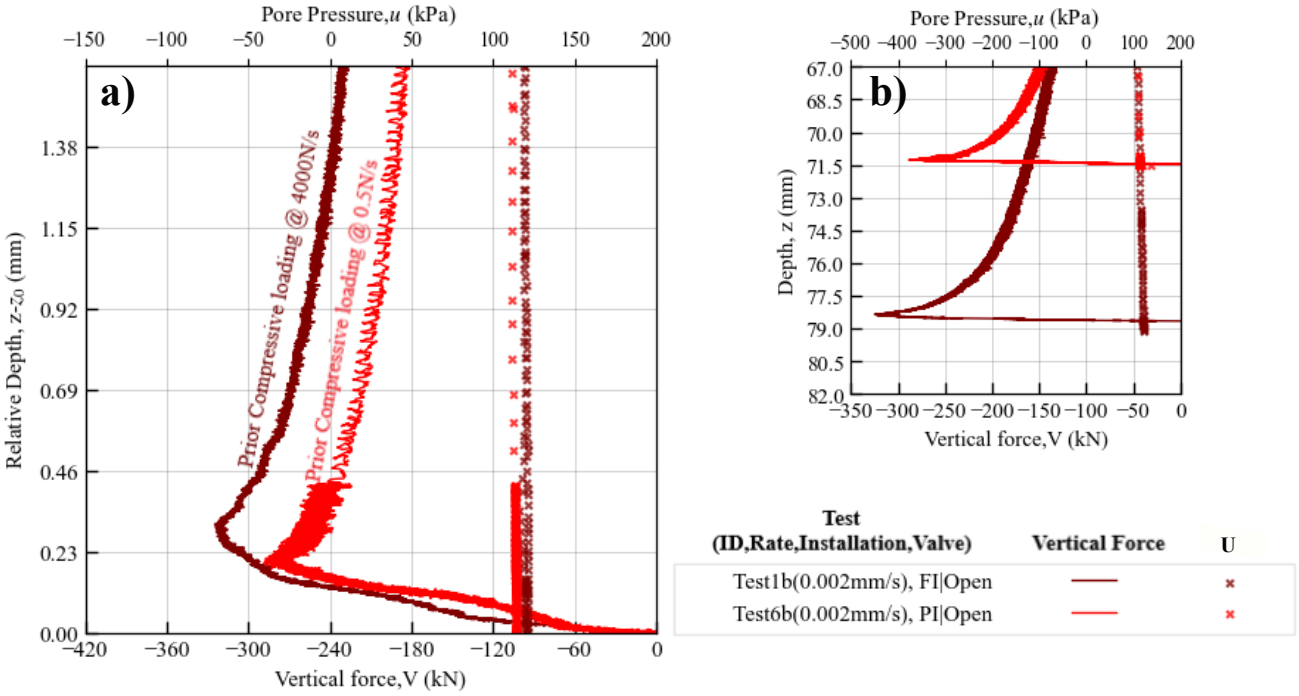

Figure 4.13: Tension with different compression history a) with relative depth, b)with depth

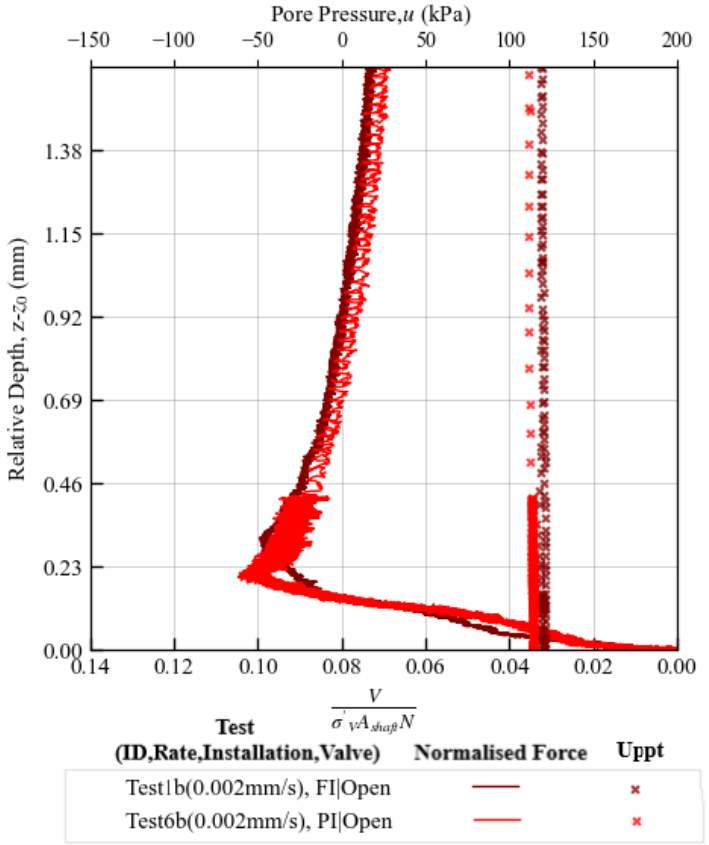

Figure 4.14: Normalized Vertical Force

Chapter 5

Conclusion

In conclusion, the research findings provide insights into the mobilized resistance and the effects of loading rates on partially installed suction caissons. Several key observations were made regarding the first research question, which examined the evolution of mobilized resistance under monotonic loading with the valve open or closed. Regardless of the installation conditions, it was found that the load transfer mechanism remained consistent, indicating similar behavior regardless of the lid contact. Additionally, when subjected to compression loading with the valve closed at a high loading rate, the capacities were similar irrespective of whether the caisson was partially or fully installed, indicating that under base filling had no significant effect. Nevertheless, when the valve was open and compression loading was applied at a slow rate, indicating a nearly drained response, the requirement of base filling was deemed essential due to the support provided by lid contact, which facilitated the mobilization of end bearing. However, when it came to tension loading, the mobilized resistance exhibited no difference whether the valve was open or closed, irrespective of the applied loading rate. This suggests that if tension is the most critical form of load that the caisson will encounter during its offshore lifetime, it may be possible to avoid underbase filling.

Regarding the second research question, which investigated the impact of loading rate on partially installed suction caissons, significant findings were discovered. In compression loading, higher loading rates led to a stiffer response and generated greater resistance compared to lower loading rates. Importantly, the mobilized resistance did not increase proportionally with the loading rates, indicating a non-linear relationship. Additionally, it was observed that as the load rate decreased, there was an increase in the dissipation of excess pore pressure, resulting in the mobilization of more shaft and tip resistance.In tension loading without any previous compressive history, it was noted that even a low loading rate of $10N/s$ could induce reverse end bearing. This suggests that the occurrence of reverse end bearing is possible and not solely reliant on the loading rate; however, the rate at which it mobilizes is influenced by the loading rate. Higher loading rates facilitated a quicker mobilization of reverse end bearing, leading to greater resistance with less displacement. However, when a compressive history was present, an increase in shaft resistance against tensile loading was observed due to the prior compression loading.

The findings enhance our understanding of suction caissons behavior, underscoring the significance of underbase filling when evaluating their response.

Chapter 6

Recommendation

This thesis only shows a part of research required to find out the actual necessity of underbase filling in suction caissons. There were many additional aspects of this research which could have be done but were avoided because of lack of time and resources. Hence following are some additional recommendation that can strengthen the argument behind the need of under base filling .

1. For the compression loading case, it will be interesting to investigate low loading rates with a closed valve and compare the response in case fully installed and partially installed suction caisson. It is evident that if a close to drained response is achieved, than full lid contact is required to mobilize end bearing capacity. However it will be interesting to know what is the load rate required to mobilize the drained response for a partially installed caisson with a closed valve. And if that load rate is possible to be faced in offshore conditions.

2. Additionally, developing a numerical model and validating it using the centrifuge results presented in this thesis would be of interest. This model could aid in the design of suction caissons without the need for under-base filling.

3. Furthermore, although this thesis focused solely on vertical monotonic loading, it is crucial to comprehend the response of partially installed suction caissons under other loading scenarios, like top moments. The behavior of the water plug under a load that induces a moment is still undetermined.

4. All the test in this thesis were monotonic loading , which are more relevant when it comes to storm loads. However, cyclic loading is more common form of loading condition observed offshore. Hence, it will be good to explore similar cases under cyclic loading.

References

DNV. (1992). *DNV CN 30.4 Foundations. Classification Notes 30.4* (Tech. Report). Høvik, Norway: DNV.

ISO. (2016). *ISO 19901-4:2016(en) Petroleum and natural gas industries — Specific requirements for offshore structures — Part 4: Geotechnical and foundation design considerations* (Standard No. ISO 19901-4).

Bienen, B., Klinkvort, R. T., O'Loughlin, C. D., Zhu, F., & Byrne, B. (2018). Suction caissons in dense sand, part i: Installation, limiting capacity and drainage. *Géotechnique*, 937–952.

Chow, S. H., Roy, A., Herduin, M., Heins, E., King, L., Bienen, B., ... Cassidy, M. (2019). *Characterisation of uwa superfine silica sand* (Tech. Rep. No. GEO 18844). Perth, Australia: The University of Western Australia.

da Silva Pereira, F., Bienen, B., & O'Loughlin, C. D. (2022). Mind the gap – an experimental study on the need for grouting suction buckets in sand under vertical cyclic loading. *Géotechnique*.

Dewoolkar, M. M., Ko, H. Y., Stadler, A. T., & Astaneh, S. M. F. (1999). A substitute pore fluid for seismic centrifuge modelling. *Geotechnical Testing Journal*, 196–210.

DNV. (2007, October). *DNV-OS-J101-2007: Det Norske Veritas. Design of offshore wind turbine structures* (Tech. Report). Det Norske Veritas.

DNV. (2022). *Energy transition outlook 2022: A global and regional forecast to 2050.*

European Commission. (2022). *2050 Long-Term Strategy.*

Eurostat. (2020). *Eurostat statistics explained.* `https://ec.europa.eu/eurostat/statistics`.

Houlsby, B. B., G.T. (2005a). Design procedures for installation of suction caissons in clay and other soils. *Institution Civil Engineers, Geotechnical Engineering*, 57–66.

Houlsby, B. B., G.T. (2005b). Design procedures for installation of suction caissons in sand. *Institution Civil Engineers, Geotechnical Engineering*, *158*, 43–56.

Kaldellis, J. K. (2022). Wind energy. In *Comprehensive renewable energy* (Second ed.). Elsevier.

Kay, S., Gourvenec, S., Palix, E., & Alderlieste, E. (2021). *Intermediate Offshore Foundations*. Publisher Name.

Lembrechts, S. (2013). *Optimization of a suction pile foundation: Initial top plate bearing of a suction pile* (Master's thesis). Delft University of Technology.

Mana, D. S. K., Gourvenec, S., & Randolph, M. F. (2013). Experimental investigation of reverse end bearing of offshore shallow foundations. *Canadian Geotechnical Journal*, 1022–1033.

Ng, C. (2014, 01). The state-of-the-art centrifuge modelling of geotechnical problems at hkust. *Journal of Zhejiang University SCIENCE A*, 1-21.

Niklas. (2022). *What are the dimensions of a wind turbine?*

OWA. (2019). *Suction installed caisson foundations for offshore wind: Design guidelines.*

Randolph, G. S., M. (2017). *Offshore geotechnical engineering*. CRC Press.

Randolph, M. F., Jewell, R. J., Stone, K. J. L., & Brown, T. A. (1991). Establishing a new centrifuge facility. In H.-Y. Ko & F. G. McLean (Eds.), *Proceedings of centrifuge 1991* (pp. 2–9). Rotterdam, the Netherlands: A. A. Balkema.

Senders, M. (2008). Suction caissons in sand as tripod foundations for offshore wind turbine. *Master Thesis*.

Stapelfeldt, M., Bienen, B., & Grabe, J. (2020). The influence of the drainage regime on the installation and the response to vertical cyclic loading of suction caissons in dense sand. *Ocean Engineering*, 107105.

Sturm, H. (2019). *Computational geomechanics*. Oslo, Norway: Norwegian Geotechnical Institute (NGI).

Tan, T. S., & Scott, R. F. (1985). Centrifuge scaling considerations for fluid-particle systems. *Géotechnique*, 461–470.

Taylor, R. (1987). Discussion of 'tan, t.-s. and scott, r.f. (1985). centrifuge scaling considerations for fluid-particle systems'. *Géotechnique*, 131–133.

Tran, M. N. (2007). Suction caissons: A new offshore foundation concept. *Australian Geomechanics*.

Tran, M. N., Randolph, M. F., & Airey, D. W. (2004). Experimental study of suction installation of caissons in dense sand. In *23rd international conference on offshore mechanics and arctic engineering, volume 1, parts a and b*.

World Economic Forum. (2022). *Europe's energy crisis: What's behind the gas price surge and how to mitigate it.*

Worldometer. (2023). *World population clock.* `https://www.worldometers.info/world-population/`. (Website)

Xie, L., Ma, S., & Lin, T. (2020). Seepage and soil plug formation in suction caissons in sand using visual tests. *Applied Sciences*, 566.

Xie, M., & Lopez-Querol, S. (2021). Numerical simulations of the monotonic and cyclic behaviour of offshore wind turbine monopile foundations in clayey soils. *Journal of Marine Science and Engineering*, 1036.

Zhang, W. (2020). *Centrifuge modelling of the behaviour of buried pipelines subjected to submarine landslides.*

Ørsted. (2020). *1991 to 2001: The first offshore wind farms.*

Ørsted. (2022). *Ørsted and northumbrian water announce a world first renewable hydrogen production facility.*

Appendix

Difference in relative densities of two boxes can be confirmed by stiffness response difference in following graphs. Showing the pressure drop developed in a tension loading case with open valve.

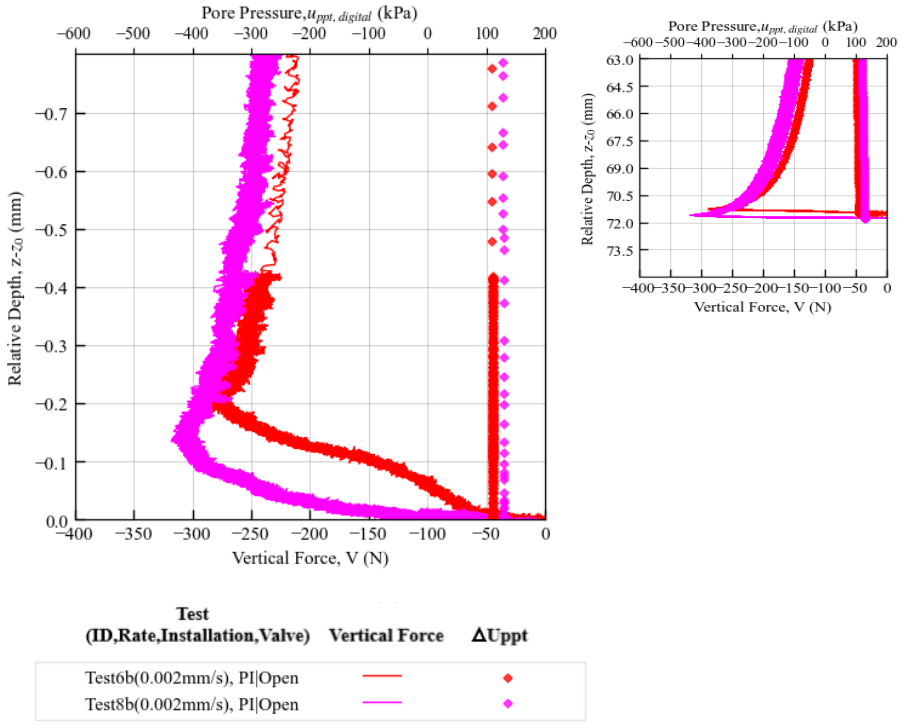

Figure 6.1: Relative density difference in strongbox a) with Relative depth, b)with depth

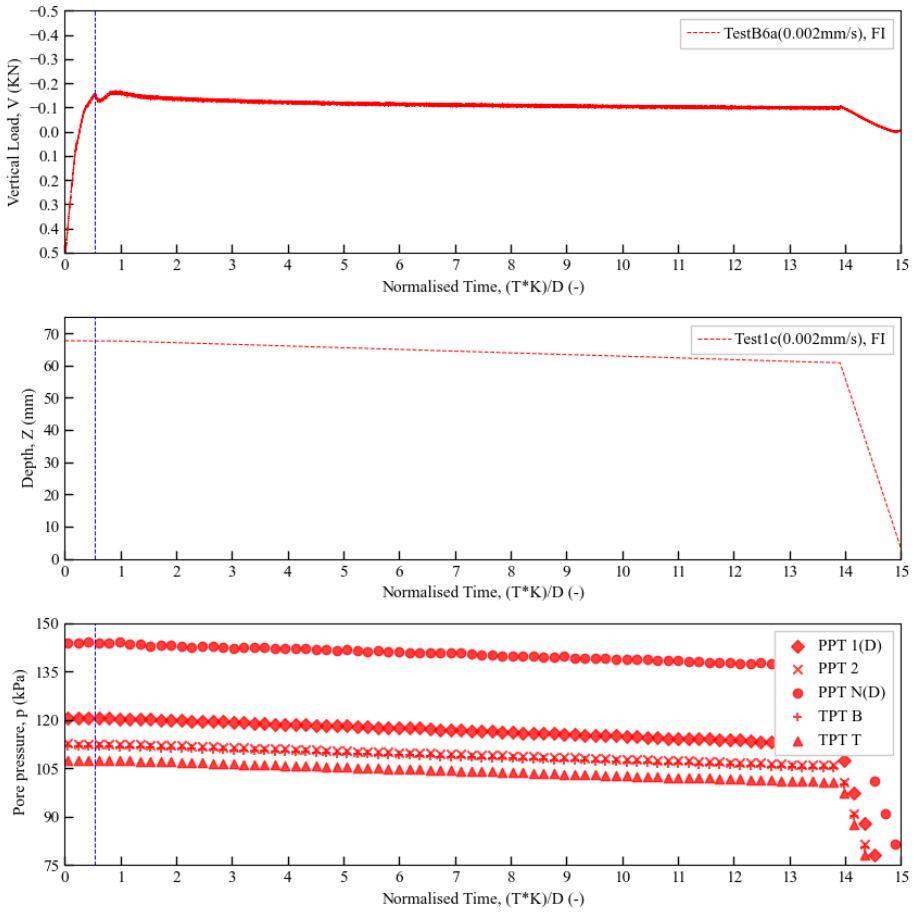

Figure 6.2: Test 1c

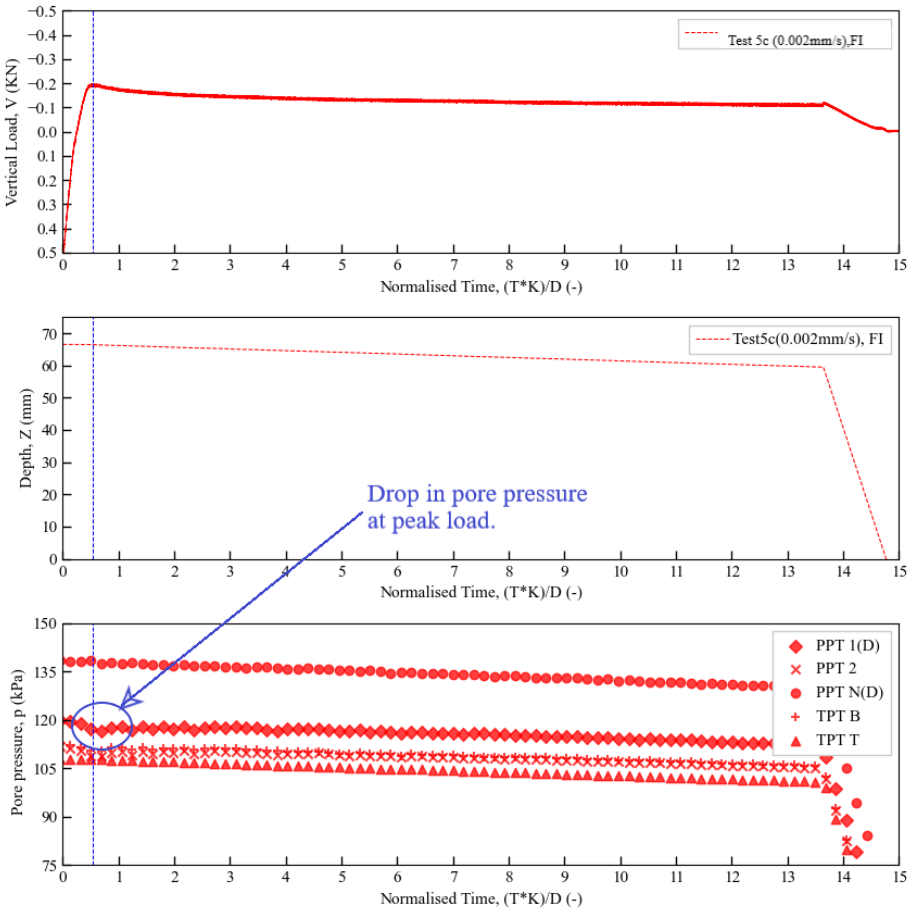

Figure 6.3: Test 5c

In [2]:
```
#Importing libraries
import pandas as pd
import numpy as np
import matplotlib.pyplot as plt
rc = {"font.family" : "serif",
      "mathtext.fontset" : "stix"}
plt.rcParams.update(rc)
plt.rcParams["font.serif"] = ["Times New Roman"] + plt.rcParams["font.serif"]
plt.rcParams['text.usetex'] = False
```

In [3]:
```
# Files and figures path
#files_path = 'C:\\Users\\Astha Sharma\\OneDrive - DEME\\Australia\\UWA Tests'
files_path = 'C:\\Users\\0030558\\OneDrive - DEME\\Australia\\UWA Tests'
fig_path = 'C:\\Users\\0030558\\OneDrive - DEME\\Australia\\UWA Tests'
```

In [4]:
```
# Importing dataframes
#trial = pd.read_csv(files_path+'\\'+'Trial'+'.txt', sep='\t')
test1a = pd.read_csv(files_path+'\\'+'Test1A'+'.txt', sep='\t')
test2a = pd.read_csv(files_path+'\\'+'Test2A'+'.txt', sep='\t')
test3a = pd.read_csv(files_path+'\\'+'Test3A'+'.txt', sep='\t')
test4a = pd.read_csv(files_path+'\\'+'Test4A'+'.txt', sep='\t')
test5a = pd.read_csv(files_path+'\\'+'Test5A'+'.txt', sep='\t')
test6a = pd.read_csv(files_path+'\\'+'Test6A'+'.txt', sep='\t')
test7a = pd.read_csv(files_path+'\\'+'Test7A'+'.txt', sep='\t')
```

In [5]:
```
# Renaming columns names
test1a.rename({' Time': 'Time', '[DONNA / LC 5kN]': 'V', '[DONNA / LC 5kN]': 'V', '[DONNA / 3]': 't_tpt', '[DONNA / 4]': 'ppt1', '[DONNA / 2]': 'ppt2',
               '[DONNA / 1]': 'b_tpt', '[PDAQ2 / N1]': 'n_ppt', '[NORAH / LDT]': 'z', '[NORAH / SYR PT]': 'sy_ppt',
               '[PACS_FB / VALVE Disp]': 'FB_motor', '[PACS_FB / DISP_Pump]': 'sy_disp', '[PACS_SP / V_LOAD]': 'SP_load',
               '[PACS_FB / V_LOAD]': 'FB_load', '[PACS_FB / V Disp]': 'z_PACS', '[PACS_SP / V Disp]': 'target_z',
               '[ / Current G]' : 'g', '[NORAH / T1]' : 'temp1', '[DONNA / T2]' : 'temp2'}, axis=1, inplace=True)
test2a.rename({' Time': 'Time', '[NORAH / LC 5kN]': 'V', '[NORAH / 3]': 't_tpt', '[ / 4]': 'ppt1', '[NORAH / 2]': 'ppt2',
               '[NORAH / 1]': 'b_tpt', '[ / N1]': 'n_ppt', '[NORAH / LDT]': 'z', '[NORAH / SYR]': 'sy_ppt',
               '[PACS_FB / VALVE Disp]': 'FB_motor', '[PACS_FB / DISP_Pump]': 'sy_disp', '[PACS_SP / V_LOAD]': 'SP_load',
               '[PACS_FB / V_LOAD]': 'FB_load', '[PACS_FB / V Disp]': 'z_PACS', '[PACS_SP / V Disp]': 'target_z',
               '[ / Current G]' : 'g', '[NORAH / T1]' : 'temp1', '[NORAH / T2]' : 'temp2'}, axis=1, inplace=True)
test3a.rename({' Time': 'Time', '[NORAH / LC 5kN]': 'V', '[NORAH / 3]': 't_tpt', '[ / 4]': 'ppt1', '[NORAH / 2]': 'ppt2',
               '[NORAH / 1]': 'b_tpt', '[ / N1]': 'n_ppt', '[NORAH / LDT]': 'z', '[NORAH / SYR]': 'sy_ppt',
               '[PACS_FB / VALVE Disp]': 'FB_motor', '[PACS_FB / DISP_Pump]': 'sy_disp', '[PACS_SP / V_LOAD]': 'SP_load',
               '[PACS_FB / V_LOAD]': 'FB_load', '[PACS_FB / V Disp]': 'z_PACS', '[PACS_SP / V Disp]': 'target_z',
               '[ / Current G]' : 'g', '[NORAH / T1]' : 'temp1', '[NORAH / T2]' : 'temp2'}, axis=1, inplace=True)
```

```
               '[ / Current G]' : 'g', '[NORAH / T1]' : 'temp1', '[NORAH / T2]' : 'temp2'}, axis=1, inplace=True)
test4a.rename({' Time': 'Time', '[NORAH / LC 5kN]': 'V', '[NORAH / 3]': 't_tpt', '[ / 4]': 'ppt1', '[NORAH / 2]': 'ppt2',
               '[NORAH / 1]': 'b_tpt', '[ / N1]': 'n_ppt', '[NORAH / LDT]': 'z', '[NORAH / SYR]': 'sy_ppt',
               '[PACS_FB / VALVE Disp]': 'FB_motor', '[PACS_FB / DISP_Pump]': 'sy_disp', '[PACS_SP / V_LOAD]': 'SP_load',
               '[PACS_FB / V_LOAD]': 'FB_load', '[PACS_FB / V Disp]': 'z_PACS', '[PACS_SP / V Disp]': 'target_z',
               '[ / Current G]' : 'g', '[NORAH / T1]' : 'temp1', '[NORAH / T2]' : 'temp2'}, axis=1, inplace=True)
test5a.rename({' Time': 'Time', '[NORAH / LC 5kN]': 'V', '[NORAH / 3]': 't_tpt', '[ / 4]': 'ppt1', '[NORAH / 2]': 'ppt2',
               '[NORAH / 1]': 'b_tpt', '[ / N1]': 'n_ppt', '[NORAH / LDT]': 'z', '[NORAH / SYR]': 'sy_ppt',
               '[PACS_FB / VALVE Disp]': 'FB_motor', '[PACS_FB / DISP_Pump]': 'sy_disp', '[PACS_SP / V_LOAD]': 'SP_load',
               '[PACS_FB / V_LOAD]': 'FB_load', '[PACS_FB / V Disp]': 'z_PACS', '[PACS_SP / V Disp]': 'target_z',
               '[ / Current G]' : 'g', '[NORAH / T1]' : 'temp1', '[NORAH / T2]' : 'temp2'}, axis=1, inplace=True)
test6a.rename({' Time': 'Time', '[NORAH / LC 5kN]': 'V', '[NORAH / 3]': 't_tpt', '[ / 4]': 'ppt1', '[NORAH / 2]': 'ppt2',
               '[NORAH / 1]': 'b_tpt', '[ / N1]': 'n_ppt', '[NORAH / LDT]': 'z', '[NORAH / SYR]': 'sy_ppt',
               '[PACS_FB / VALVE Disp]': 'FB_motor', '[PACS_FB / DISP_Pump]': 'sy_disp', '[PACS_SP / V_LOAD]': 'SP_load',
               '[PACS_FB / V_LOAD]': 'FB_load', '[PACS_FB / V Disp]': 'z_PACS', '[PACS_SP / V Disp]': 'target_z',
               '[ / Current G]' : 'g', '[NORAH / T1]' : 'temp1', '[NORAH / T2]' : 'temp2'}, axis=1, inplace=True)
test7a.rename({' Time': 'Time', '[NORAH / LC 5kN]': 'V', '[NORAH / 3]': 't_tpt', '[ / 4]': 'ppt1', '[NORAH / 2]': 'ppt2',
               '[NORAH / 1]': 'b_tpt', '[ / N1]': 'n_ppt', '[NORAH / LDT]': 'z', '[NORAH / SYR]': 'sy_ppt',
               '[PACS_FB / VALVE Disp]': 'FB_motor', '[PACS_FB / DISP_Pump]': 'sy_disp', '[PACS_SP / V_LOAD]': 'SP_load',
               '[PACS_FB / V_LOAD]': 'FB_load', '[PACS_FB / V Disp]': 'z_PACS', '[PACS_SP / V Disp]': 'target_z',
               '[ / Current G]' : 'g', '[NORAH / T1]' : 'temp1', '[NORAH / T2]' : 'temp2'}, axis=1, inplace=True)
```

In [6]:
```
test1a.n_ppt = test1a.n_ppt
test1a.ppt1 = test1a.ppt1
test2a.n_ppt = test2a.n_ppt
test2a.ppt1 = test2a.ppt1
test3a.n_ppt = test3a.n_ppt
test3a.ppt1 = test3a.ppt1
test4a.n_ppt = test4a.n_ppt
test4a.ppt1 = test4a.ppt1
test5a.n_ppt = test5a.n_ppt
test5a.ppt1 = test5a.ppt1
test5a.z = test5a.z*-1 #so it has the same sign as the others
test6a.n_ppt = test6a.n_ppt
test6a.ppt1 = test6a.ppt1
test6a.z = test6a.z*-1 #so it has the same sign as the others
test7a.n_ppt = test7a.n_ppt
test7a.ppt1 = test7a.ppt1
test7a.z = test7a.z*-1 #so it has the same sign as the others
```

In [7]:
```
#PLOTING VERTICAL LOAD AGAINST TIME
fig, ax = plt.subplots(figsize=(6,6))
file_name = 'Vertical load'

# Ploting box A

x1 = (test1a.Time)
y1 = (test1a.V)/1000

ax.plot (x1[1:82210], y1[1:82210], color='blue', label="Test1a(0.002mm/s), PI|Open", linewidth=0.75, linestyle="-")
ax.plot (x1[82210:], y1[82210:], color='red', label="Test1b(0.002mm/s), FI|Open", linewidth=0.75, linestyle="-")

sec = x1[22660]

print (sec)

depth = y1[22660]

print ('Embedment depth',(depth))


# Identify the coordinates of the peak point
max_idx = np.argmax(y1)
max_y1 = y1[max_idx]
max_x1 = x1[max_idx]

print(f"Peak coordinates: ({max_x1}, {max_y1})")


# plots the peak point
#plt.grid(color='grey', linestyle='-', linewidth=0.5)


ax.tick_params(direction='in', length=6, width=1, colors='black',
               grid_color='black', labelsize=11, grid_alpha=0.5)
plt.xticks(np.arange(0, 15e3+1, 1.5e3))
plt.yticks(np.arange(-1, 9, 0.5))
plt.xlabel(" Time, T (sec)", fontsize=11)
ax.xaxis.tick_bottom()
ax.xaxis.set_label_position('bottom')
ax.set_xlim(0, 15e3)
ax.set_ylim(-1, 8)
plt.ylabel(" Vertical Load, V (kN)", fontsize=12)
```

In [8]:
```
#PLOTING VERTICAL LOAD AGAINST TIME
fig, ax = plt.subplots(figsize=(8.6,8.6))
file_name = 'Vertical load'

# Ploting box A

x1 = (test1a.Time)
y1 = (test1a.V)/1000
x2 = (test5a.Time)
y2 = (test5a.V)/1000

ax.plot (x1, y1, color='blue', label="TestA1a", linewidth=0.75, linestyle="--")
ax.plot (x2, y2, color='black', label="TestA5a", linewidth=0.75, linestyle="--")

sec = x1[22660]

print (sec)

depth = y1[22660]

print ('Embedment depth',(depth))


# Identify the coordinates of the peak point
max_idx = np.argmax(y1)
max_y1 = y1[max_idx]
max_x1 = x1[max_idx]

print(f"Peak coordinates: ({max_x1}, {max_y1})")


# plots the peak point
plt.grid(color='grey', linestyle='-', linewidth=0.5)


ax.tick_params(direction='in', length=6, width=1, color='black',
               grid_color='black', labelsize=11, grid_alpha=0.5)
plt.xticks(np.arange(0, 15e3+1, 1.5e3))
plt.yticks(np.arange(-1, 9, 0.5))
plt.xlabel(" Time, T (sec)", fontsize=12)
ax.xaxis.tick_bottom()
ax.xaxis.set_label_position('bottom')
ax.set_xlim(0, 15e3)
ax.set_ylim(-1, 8)
plt.ylabel(" Vertical Load, V (KN)", fontsize=12)
```

Functions

In [10]:
```
# Function to calculate suction pressure at lid invert and stress
def calc_excess_pwp_and_stress (df):

    df['excess_pwp1'] = df.ppt1 - df.t_tpt - (df.ppt1.iloc[0] - df.t_tpt.iloc[0])
    df['excess_pwp2'] = df.ppt2 - df.t_tpt - (df.ppt2.iloc[0] - df.t_tpt.iloc[0])
    df['excess_pwp3'] = df.b_tpt - df.t_tpt - (df.b_tpt.iloc[0] - df.t_tpt.iloc[0])
    df['excess_n'] = df.n_ppt - df.t_tpt - (df.n_ppt.iloc[0] - df.t_tpt.iloc[0])
    df['V_stress'] = (df.V)/1000/(np.pi*0.08*0.08/4)
    df['V1']= ((df.V[92455:])-(((-1*df.z[92455:])-14.984)/0.00437))/1000
    df['VNF'] =  (df.V)/((-1*df.z)*(-1*df.z)*0.0201062*100)
    df['Time'] =(df.Time)#*0.37875e-2
    #df['delta_z'] = df.z.diff()
    #df['delta_V_stress'] = df.V_stress.diff()
    #df['delta_Time'] = df.Time.diff()

    return
```

In [11]:
```
#function to find out starting time
def finding_start_time(df,limit_index, limit_load, limit_Time, first_point):
    fig, ax = plt.subplots(nrows=1, ncols=2, figsize=(8,4), sharey=False)


    df1 = df[df.index < first_point] #defining points before touch down
    df2 = df[df.index > first_point] #difinig point after touch down

    # Ploting index vs load - in theory where the stress increases is the touch down point
    ax[0].scatter (df1.index,df1.V, s=1)
    ax[0].scatter (df2.index,df2.V, s=1)
    ax[0].set_xlim(limit_index)
    ax[0].set_ylim(limit_load)
    ax[0].set_xlabel('Index', fontsize=11)
    ax[0].set_ylabel('load, $\mathit{(V)}$ (N)', fontsize=11)


    # Ploting stress vs displacement - this gives confidence that the chosen point makes sense in stress displacement
    ax[1].scatter (df1.index,df1.Time, s=1)
    ax[1].scatter (df2.index,df2.Time, s=1)
    ax[1].set_xlim(limit_index)
    ax[1].set_ylim(limit_Time)
    ax[1].set_xlabel('Index', fontsize=11)
    ax[1].set_ylabel('Time, $\mathit{t}$ (s)', fontsize=11)
```

In [12]:
```
# Fucntion to correct initial time
def correct_time (df, first_point):
    df.Time = df.Time - np.asarray(df.Time[df.index == first_point])
```

In [13]:
```
# Fuction to find touch-down depth
def touch_down_depth (df, limit_index, limit_stress, limit_z, first_point):

    fig, ax = plt.subplots(nrows=1, ncols=2, figsize=(8,4), sharey=False)

    df1 = df[df.index < first_point] #defining points before touch down
    df2 = df[df.index > first_point] #difinig point after touch down

    # Ploting index vs stress - in theory where the stress increases is the touch down point
    ax[0].scatter (df1.index, df1.V_stress)
    ax[0].scatter (df2.index, df2.V_stress)
    ax[0].set_xlim(limit_index)
    ax[0].set_ylim(limit_stress)
    ax[0].set_ylabel('Stress, $\mathit{(V/A)}$', fontsize=11)
    ax[0].set_xlabel('Index', fontsize=11)


    # Ploting stress vs displacement - this gives confidence that the chosen point makes sense in stress displacement
    ax[1].scatter (df1.index, df1.z)
    ax[1].scatter (df2.index, df2.z)
    ax[1].set_xlim(limit_index)
    ax[1].set_ylim(limit_z)
    ax[1].set_xlabel('Index', fontsize=11)
    ax[1].set_ylabel('Depth, $\mathit{z}$ (mm)', fontsize=11)
```

In [14]:
```
# Fucntion to correct initial depth
def correct_depth (df, first_point):
    df.z = df.z - np.asarray(df.z[df.index == first_point])
    df.z_PACS = df.z_PACS - np.asarray(df.z_PACS[df.index == first_point])
```

In [14]:
```
# Fucntion to correct initial depth
def correct_depth (df, first_point):
    df.z = df.z - np.asarray(df.z[df.index == first_point])
    df.z_PACS = df.z_PACS - np.asarray(df.z_PACS[df.index == first_point])
```

In [15]:
```
# Load rate and displacement rate
def rates (df):

    i=1
    last_i = df.last_valid_index()
    df['z_rate'] = df.V*0
    df['V_stress_rate'] = df.V*0
    df['sy_rate'] = df.V*0
    z_rate=df.V*0 #setting z_rate as a column with zeros
    V_stress_rate=df.V*0 #setting load rate as a column with zeros
    sy_rate=df.V*0 #setting load rate as a column with zeros

    while i <= last_i:
        z_rate.iloc[i]=(df.z_PACS.iloc[i]-df.z_PACS.iloc[i-1])/(df.Time.iloc[i]-df.Time.iloc[i-1])
        V_stress_rate.iloc[i]=(df.V_stress.iloc[i]-df.V_stress.iloc[i-1])/(df.Time.iloc[i]-df.Time.iloc[i-1])
        sy_rate.iloc[i]=(df.sy_disp.iloc[i]-df.sy_disp.iloc[i-1])/(df.Time.iloc[i]-df.Time.iloc[i-1])

        i = i + 1

    z_rate = z_rate.rolling(window=10*5, min_periods=1).mean()
    V_stress_rate = V_stress_rate.rolling(window=10*5, min_periods=1).mean()
    sy_rate = sy_rate.rolling(window=10*5, min_periods=1).mean()
    df['z_rate'] = z_rate
    df['V_stress_rate'] = V_stress_rate
    df['sy_rate'] = sy_rate
```

In [16]:
```
def find_approximate_indexes(dataset, approximate_value, tolerance):
    indexes = [i for i, x in enumerate(dataset) if abs(x - approximate_value) <= tolerance]
    return indexes
```

Initial processing

In [17]:
```
# Calculating suction pressure at lid invert, stress and rates
#calc_excess_pwp_and_stress (trial)
calc_excess_pwp_and_stress (test1a)
calc_excess_pwp_and_stress (test2a)
calc_excess_pwp_and_stress (test3a)
calc_excess_pwp_and_stress (test4a)
calc_excess_pwp_and_stress (test5a)
calc_excess_pwp_and_stress (test6a)
calc_excess_pwp_and_stress (test7a)
```

In [18]:
```
#finding Intial time

finding_start_time (test6a, [109395,109400], [600, -500], [455, 0], 109399)
```

In [21]:
```
# Compression and tension start and peak index
testA1a_start= 22660
testA2a_start= 102196
testA3a_start= 91284
testA4a_start= 149618
testA5a_start= 90450
testA6a_start= 92455
testA7a_start= 95374
testA1b_start= 82210
testA2b_start= 107260
testA3b_start= 98599
testA4b_start= 203320
testA5b_start= 293840
testA6b_start= 100690
testA7b_start= 139615
testA1a_peak= 69983
testA2a_peak= 102269
testA3a_peak= 91612
testA4a_peak= 149782
testA5a_peak= 217516
testA6a_peak= 92539
testA7a_peak= 95458
testA1b_peak= 149300
testA2b_peak= 107340
testA3b_peak= 98680
testA4b_peak= 203520
testA5b_peak= 294215
testA6b_peak= 118310
testA7b_peak= 121083
```

In [22]:
```
# Finding touch-down depth:
## try diferent values for 'first _point'
touch_down_depth (test1a, [10000, 0], [-5, 25], [-10, 10], 3030)
```

In [23]:
```
# Correcting initial depth - Only run once for each test otherwise it will keep changing the initial depth
correct_depth (test1a, 1025)
correct_depth (test2a, 1620)
correct_depth (test3a, 4100)
correct_depth (test4a, 4800)
correct_depth (test5a, 1650)
correct_depth (test6a, 4380)
correct_depth (test7a, 3010)
```

In [24]:
```
#Corrected Initial time
correct_time (test1a,22660)
correct_time (test2a,102196)
correct_time (test3a,91284)
correct_time (test4a,149618)
correct_time (test5a,90450)
correct_time (test6a,92455)
correct_time (test7a,95375)
```

In [1]:

```
# Test name and labels
TestA1a = "Test1a(0.002mm/s), PI|Open"
TestA1b = "Test1b(0.002mm/s), FI|Open"
TestA2a = "Test2a(3mm/s), PI|Close"
TestA2b = "Test2b(3mm/s), PI|Close"
TestA3a = "Test3a(500N/s), PI|Close"
TestA3b = "Test3b(3mm/s), PI|Close"
TestA4a = "Test4a(2000N/s), PI|Close"
TestA4b = "Test4b(500N/s), PI|Close"
TestA5a = "Test5a(0.002mm/s), FI|Open"
TestA5b = "Test5b(250N/s),FI|Close"
TestA6a = "Test6a(4000N/s), PI|Close"
TestA6b = "Test6b(0.002mm/s), PI|Open"
TestA7a = "Test7a(4000N/s), FI|Close"
TestA7b = "Test7b(50N/s), FI|Close"
PPT1 = "$u_{ppt, digital}$"
PPT2 = "$u_{ppt, analog}$"
PPTN ="$u_{ppt, needle}$"
TPTT = "$u_{tpt, top}$"
TPTB ="$u_{tpt, bottom}$"
EPPT1 = "Excess Pore Pressure,$\Delta u_{ppt, digital}$"
EPPT2 = "Excess Pore Pressure,$\Delta u_{ppt, analog}$"
EPPTN ="Excess Pore Pressure,$\Delta u_{ppt, needle}$"
EPPT = "Excess Pore Pressure,$\Delta u_{ppt}$"
ppt1 = "Pore Pressure,$u_{ppt, digital}$ (kPa)"
ppt2 = "Pore Pressure,$u_{ppt, analog}$ (kPa)"
pptn = "Pore Pressure,$u_{ppt, needle}$ (kPa)"
ppt = "Pore Pressure,$u_{ppt}$ (kPa)"
VF = "Vertical force,V (kN)"
NVF = "$\\frac{ V}{ z\\gamma_{sat}A_{shaft}N} \\times 100 {}$  (%)"
FR = "$\\frac{ V}{ \\sigma'_{V}A_{shaft}N} \\ {}$  "
D = "Depth, z (mm)"
RD = "Relative Depth, z-$z_{0}$ (mm)"
print(NVF)
```

```
$\frac{ V}{ z\gamma_{sat}A_{shaft}N} \times 100 {}$  (%)
```

Graphs